LAWRENCE
LIVERMORE
NATIONAL
LABORATORY

LLNL-TH-434077

Synthesis, Consolidation and Characterization of Sol-gel Derived Tantalum-Tungsten Oxide Thermite Composites

O. Cervantes

June 4, 2010

Disclaimer

This work performed under the auspices of the U.S. Department of Energy by Lawrence Livermore National Laboratory under Contract DE-AC52-07NA27344.

Synthesis, Consolidation and Characterization of Sol-gel Derived Tantalum-Tungsten Oxide Thermite Composites

By

Octavio Cervantes

B.S. (California State University, Northridge) 2000
M.S. (University of Illinois at Urbana-Champaign) 2002

DISSERTATION

Submitted in partial satisfaction of the requirements for the degree of

DOCTOR OF PHILOSOPHY

in

MATERIALS SCIENCE & ENGINEERING

in the

OFFICE OF GRADUATE STUDIES

of the

UNIVERSITY OF CALIFORNIA

DAVIS

Approved:

_____
Zuhair A. Munir, Chair

_____
James F. Shackelford

_____
Subhash Risbud

Committee in Charge

2010

Synthesis, Consolidation and Characterization of Sol-gel Derived Tantalum-Tungsten Oxide Thermite Composites

ABSTRACT

Energetic composite powders consisting of sol-gel (SG) derived nanostructured tungsten oxide were produced with various amounts of micrometer-scale tantalum fuel metal. Such energetic composite powders were ignition-tested and results show that the powders are not sensitive to friction, spark and/or impact ignition. Initial consolidation experiments, using the High Pressure Spark Plasma Sintering (HPSPS) technique, on the SG derived nanostructured tungsten oxide produced samples with higher relative density than can be achieved with commercially available tungsten oxide. The SG derived nanostructured tungsten oxide with immobilized tantalum fuel metal (Ta - WO_3) energetic composite was consolidated to a density of 9.17 $g \cdot cm^{-3}$ or 93% relative density. In addition, those samples were consolidated without significant pre-reaction of the constituents, thus retaining their stored chemical energy.

The heat of combustion of two distinctly synthesized stoichiometric tantalum-tungsten oxide energetic composites was investigated by bomb calorimetry. One composite was synthesized using a sol-gel (SG) derived method in which micrometric-scale tantalum is immobilized in a tungsten oxide three-dimensional nanostructured network structure. The second energetic composite was made from the mixing of micrometric-scale tantalum and commercially available (CA) nanometric tungsten oxide powders. The energetic

composites were consolidated using the spark plasma sintering (SPS) technique under a 300 MPa pressure and at temperatures of 25, 400, and 500°C. For samples consolidated at 25°C, the density of the CA composite is 61.65 ± 1.07% in comparison to 56.41 ± 1.19% for the SG derived composite. In contrast, the resulting densities of the SG composite are higher than the CA composite for samples consolidated at 400 and 500°C. The theoretical maximum density for the SG composite consolidated to 400 and 500°C are 81.30 ± 0.58% and 84.42 ± 0.62%, respectively. The theoretical maximum density of the CA composite consolidated to 400 and 500°C are 74.54 ± 0.80% and 77.90 ± 0.79%, respectively. X-ray diffraction analyses showed an increase of pre-reaction of the constituents with an increase in the consolidation temperature. The increase in pre-reaction results in lower stored energy content for samples consolidated to 400 and 500°C in comparison to samples consolidated at 25°C.

The activation energy of a SG derived tantalum-tungsten oxide thermite composite was determined using the Kissinger isoconversion method. The SG derived powder was consolidated using the HPSPS technique at 300 and 400°C. The ignition temperatures were investigated under high heating rates (500 – 2000°C·min^{-1}). Such heating rates were required in order to ignite the thermite composite. Samples consolidated at 300°C exhibit an abrupt change in temperature response prior to ignition of the main combustion reaction. This change in temperature response is attributed to the crystallization of the amorphous WO_3 in the SG derived Ta-WO_3 thermite composite and not to a pre-

ignition reaction between the constituents. Ignition temperatures for the Ta-WO_3 thermite ranged from approximately 465 to 670°C. The activation energies of the SG derived Ta-WO_3 thermite composite consolidated at 300 and 400°C were determined to be 37.787 ± 1.58 $kJ \cdot mol^{-1}$ and 57.381 ± 2.26 $kJ \cdot mol^{-1}$, respectively.

Pa’ mi esposa Rebeca Vasquez y mis hijos
Diego Octavio Cervantes, Santiago Octavio Cervantes
y … Si Dios quiere!!

“La Humildad es la Riquesa mas Grande del Mundo”
O.G. Cervantes, 2010

ACKNOWLEDGEMENTS

There are many individuals who have helped me make this dissertation possible that I would be impossible to list them all, but most importantly, I would like to thank God for allowing me to accomplish this academic endeavor and for his spiritual guidance throughout this process.

I am truly thankful to Distinguished Prof. Zuhair A. Munir for his support as a mentor, colleague and friend. I could not have accomplished this work without his insightful advice. I would like to thank my qualifying and dissertation committees: Prof. James F. Shackelford, Prof. Subhash Risbud, Prof. Joanna Groza and Prof. Umberto Anselmi-Tamburini (University of Pavia) for their support.

I would also like to thank my supervisor, colleague, friend and principal investigator of this project, Dr. Alexander E. Gash. Without your insightful input and knowledge this dissertation project would have been more difficult. Thanks, Alex. I also want to thank my dear friend and colleague Dr. Joshua E. Kuntz for all the great discussions, crazy ideas, sage advice and assistance during this project. Thank you for your trust and for believing in me. You always kept me on my toes.

I would never have completed this dissertation without the support and love of my family. “Mis viejitos”, Juan and Medalia Cervantes who have been the true

engineers in my life and have shown me to be humble and respectful to others at all times. My siblings, Lourdes, Myrna and Victor Cervantes who I admire and respect. Their independent qualities have impacted my life in their own ways. I want to thank my “cuñados” (Cirilo Rodriguez and Antonio Garcia) and “cuñada” (Brenda Cervantes) for their help and affection. Thanks everyone for believing in me.

I truthfully and honestly want to thank my best friend and wife, Rebeca Vasquez, for all her unconditional and tireless support throughout my college career. For her kind and cheerful words of support when nothing was working in the lab. She is the pedestal of our home and this dissertation work. I love you, Amor. I also want to thank her for giving the two most beautiful boys the world has ever seen, Diego Octavio Cervantes and Santiago Octavio Cervantes. Life is much more meaningful having the three of you around.

FINANCIAL SUPPORT

This work performed under the auspices of the U.S. Department of Energy by Lawrence Livermore National Laboratory under Contract DE-AC52-07NA27344. The authors are grateful to the Joint DoD/DOE Munitions Technology Development Program for funding this project.

TABLE OF CONTENTS

CHAPTER 3

CHAPTER 4

CHAPTER 5

LIST OF FIGURES

LIST OF TABLES

Chapter 1

1.0 INTRODUCTION

1.1 ENERGETIC MATERIALS

Energetic materials are substances that store chemical energy. Energetic materials can be classified into different classes that include propellants, pyrotechnics, explosives and common fuels such as gasoline and diesel. Energetic materials are made up of a fuel and oxidizer constituents. For the most part, the energy release rate of propellants and pyrotechnics is a relatively slow (seconds scale) deflagration process. In contrast, explosives release their energy in a relative fast (microseconds) detonation process. There are several methods for producing energetic materials, some of which will be presented in Section 1.3, but the most common method is by mixing oxidizer and fuel constituents. The mixing of such constituents may produce monomolecular energetics, where the oxidizer and fuel moieties are contained within a single molecule such as nitrocellulose, nitroglycerine and trinitrotoluene or energetic composites of separate oxidizer and fuel phases.

1.2 ENERGETIC COMPOSITES

Energetic composites are of significant interest due to the wide range of material properties that can be tailored by controlling the chemical composition and the particle size of the fuel metal and oxidizer, independently. One of the

main subsets of energetic composites consists of thermite materials where typically, the fuel is a metal and the oxidizer is a metal oxide. Thermite reactions are exothermic reactions that may be initiated and become self-sustaining releasing large amounts of heat [1]. A typical thermite reaction is described in Eq. (1.1)

$$M + AO \rightarrow MO + A + \Delta H \qquad 1\text{-}1$$

where M is a metal, A is a metal oxide, MO and AO are their corresponding oxides and ΔH is the heat of reaction.

Thermite composites have been studied intensively due to the wide variety of potential applications such as demolition of concrete [2], self-destructive electrical components [3], primers [4], stab detonators [5], and reactive fragments [6]. A more thorough review of thermite reactions and their applications has been provided by Wang et al. [1].

Due to the relatively high enthalpy of formation of its oxide at 25°C (-1675.7 $kJ \cdot mol^{-1}$) and its low melting point (660°C), aluminum has been widely used as a fuel metal. Nanometric sized aluminum has been studied with a variety of oxidizers such as Fe_2O_3, Bi_2O_3, CuO, MoO_3 and WO_3. Nanometric aluminum – metal oxide thermite reactions have been shown to be highly energetic and proceed at relatively high rates. Although aluminum – metal oxide energetic composites have been widely studied, most studies have focused on reactions of loose powders, partially confined systems, or resin-bonded energetic

composite materials [7-10]. There have been comparatively few studies with alternative fuel metals such as Ta, Zr, Hf, or Si mixed with oxidizers [11]. And those studies have focused on loose powders or consolidated parts with relatively low value (< 50%) of relative density.

1.3 SYNTHESIS OF ENERGETIC COMPOSITES

As presented in Section 1.1, energetic materials may be produced by simply mixing oxidizer and fuel constituents, but there are other synthesis methods by which energetic composites may be produce. Energetic materials can be prepared as films deposited on substrates. These films may be composed of alternating metallic layers [12, 13] or layers of metal fuel and metal oxide with well defined thickness and composition [14]. A major disadvantage to this approach is that it is time consuming, expensive, and yields relatively small amounts of material.

Another method for synthesizing energetic composites involves the ultrasonic mixing of fuel and oxidizer nanoparticles. Such subset of energetic composites has been referred to as Metastable Interstitial Composites (MIC) [8]. And although, this process is relatively inexpensive and large quantities of material can be prepared quickly, an important concern is the homogeneity of the fuel and oxidizer mixture to minimize variability in their thermal behavior.

Arrested Reactive Milling (ARM) is another method by which energetic materials may be produced. In this method exothermic nano-energetic composites are prepared by mechanically milling the starting metal fuel and

metal oxide mixture but stopping the milling process before the mixture reacts exothermally [15-17].

Sol-gel synthesis [18-20] techniques have been used to produce energetic composites consisting of immobilized metal fuels inside a three-dimensional nanostructured metal oxide. This method produces an energetic composite in which the metal fuel is homogeneously distributed throughout the nanometric oxidizer, and it can be scaled up to produce large sample quantities.

1.4 CONSOLIDATION OF ENERGETIC COMPOSITES

Due to the fact that energetic composites store energy, one is required to take the necessary precautions to avoid accidents. For instance, if one wants to consolidate the energetic material, one may not apply considerable temperatures and pressures that may initiate the exothermic reaction of the composite. To minimize pre-combustion reactions between the energetic constituents during the consolidation process, most energetic composites have been pressed into pellets using conventional hydraulic presses at room temperature [7-11]. The resulting average densities of such pellets are in the order of 50% their theoretical maximum density. In order to minimize the pre-combustion reaction between the energetic constituents and increase the resulting theoretical maximum density, the spark plasma sintering (SPS) technique may be applied on the consolidation of energetic composites.

Essentially, the SPS method is based on the theory of high temperature plasma generated in the gaps between powder materials by an electrical

discharge during DC pulsing while applying pressure to the powders. The DC pulsing provides rapid Joule heating to a graphite die assembly which heats the powders of interest. Figure 1 shows a model of the SPS setup. Therefore, SPS can rapidly consolidate powders to near theoretical densities through the combined actions of a rapid heating rate and pressure application.

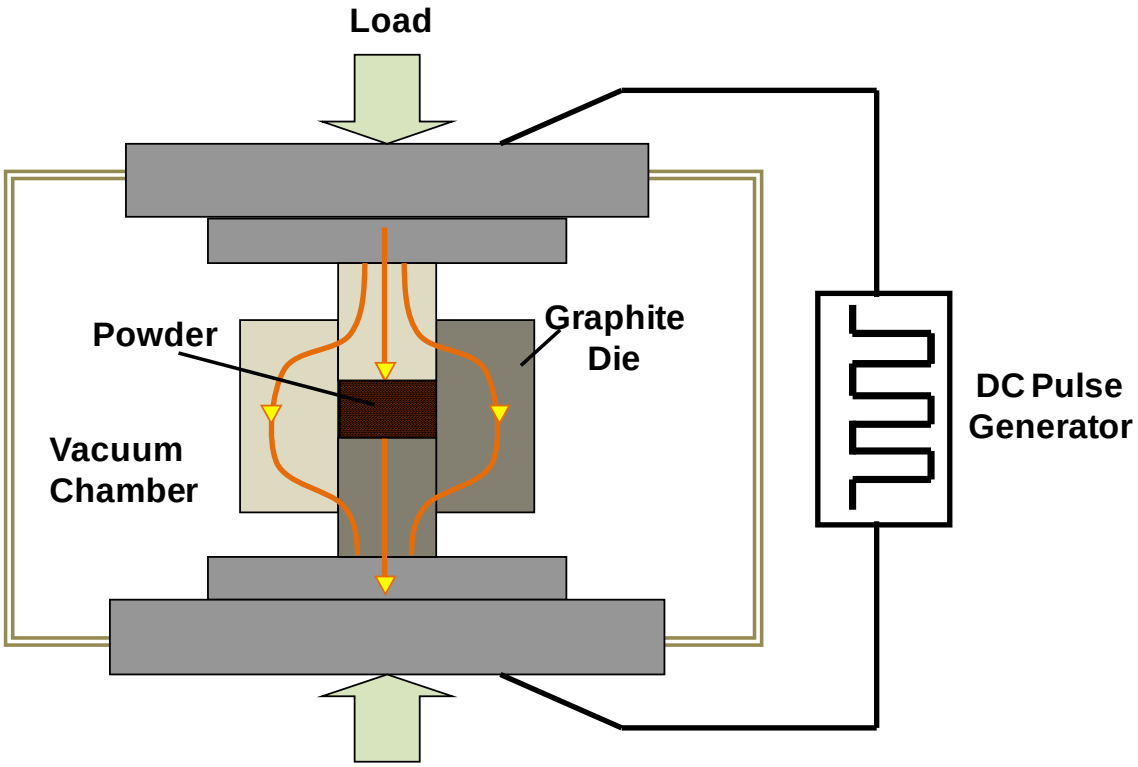

Figure 1: Schematic representation of SPS setup.

In our research, SPS is carried out under vacuum using a Dr. Sinter 1050 apparatus, Figure 2 (Sumitomo Coal Mining Co., Japan).

Figure 2: Image of the Sumitomo Mining Corp. model SPS-1050 consolidation equipment known as “Dr. Sinter”.

1.5 PERFORMANCE MEASUREMENTS

In addition to investigations on the synthesis and characterization of energetic composites, several efforts have been made to determine their performance. Several researchers have investigated the ignition sensitivity, energy release rates, and the activation energies of energetic composites as a function of fuel particle size.

Among the most common techniques to characterize the performance of energetic materials are differential scanning calorimetry (DSC) and differential thermal analysis (DTA). Several researchers [21-26] have used such techniques to measure the performance of energetic materials, but others have used or developed different techniques to measure the performance of energetic materials. Perry, et al. [27, 28] measured the ignition and propagation

characteristics of unconfined aluminum–tungsten oxide powder. During the experiment, the burning velocity of the thermite was measured using an open channel. The powder was ignited on one end of the channel and two light fibers transmitted light to optical detectors. The velocity was determined using the time between the two light pulses. In addition, Perry, et al. [27, 28] measured the pressurization rate and peak pressure by igniting the material in a closed vessel (13 cm^{-3}) and recording the pressure-time data. The powder was ignited using a fiber-optic coupled 30 ns, 20 mJ pulse Nd-YAG laser. The pressure vessel was instrumented with two pressure transducers to collect the data.

Bockmon, et al. [29] performed combustion measurements on aluminum-molybdenum oxide using open ended cylindrical acrylic tubes in which the sample is packed and ignited. The experimental setup is instrumented with fiber-optic photodetectors and piezocrystal pressure sensors to measure the combustion velocity and the pressure generated by the burning reaction.

To determine the ignition kinetics of an aluminum rich – titanium alloy which was processed by mechanical alloying the material, Shoshin, et al. [30] coated a thin layer of the powder onto an electrically heated filament. A DC voltage was applied to heat the filament. A silicon photodiode was focused on the coated sample to determine the ignition of the sample. By varying the applied voltage, Shoshin was able to apply different heating rates ranging from 10^3 to 10^4 $K \cdot s^{-1}$ to the material of interest and therefore, calculate important kinetic parameters. The temperature history of the heated filament was

measured using a high-speed, infrared pyrometer. This experimental technique has also been used in thermite composites [31].

To characterize the combustion performance of their powders produced by Arrested Reactive Milling (ARM) Schoenitz, et al. [15] and Stamatis, et al. [32] used the constant volume explosion experiments presented by Cashdollar et al. [33]. Essentially, the experiments consisted in placing the thermite powder on a ceramic support inside a closed pressure vessel equipped with a pressure transducer. The powder was then ignited using a heated wire. The pressure traces were recorded and combustion products were collected for further analysis.

In a less complex experimental setup, Lee et al. [34] determined the activation energy of several intermetallic materials from temperature-time thermograms using a conventional furnace while purging argon gas and varying heating rate.

And in a more sophisticated experimental setup, Mileham [35] characterized the reactive process that occurs during the laser initiation of an aluminum-iron oxide thermite. The reactive process was analyzed using the laser-induced desorption ionization time-of-flight mass spectrometry technique and learned that the decrease in ignition time observed in this material might be due to the liberation of reactive metallic aluminum when the particle size is small.

1.6 OBJECTIVE

The goal of this study was to synthesize a nanostructured thermite composed of amorphous WO_3 with immobilized Ta metal particles using sol-gel techniques and to consolidate the Ta-WO_3 energetic composite to near theoretical density without significant reaction to ensure complete retention of the chemical energy. To achieve densification without significant pre-combustion reaction, it is necessary to use accelerated consolidation techniques. One such technique is spark plasma sintering (SPS). The process combines the application of pulsed DC current with uniaxial pressure. Its advantages stem from a combination of factors including high heating rate (up to about 2000°C·min^{-1}), high pressure (up to about 1 GPa),and electromigration [36]. The high pressure is obtained in a modification of die design, as has been reported previously [37]. We utilized this modified SPS technique in our study, which we will refer to as High Pressure Spark Plasma Sintering (HPSPS). Chapter 2.0 will cover in detail the synthesis of the sol-gel Ta-WO_3 energetic composite as well as the consolidation conditions used to densify the composite.

Aside from synthesizing and consolidating an amorphous WO_3 with immobilized Ta thermite composite, it is important to evaluate the performance of the thermite composite. Chapter 3.0 will report on the energy release of the consolidated composite pellets determined by combustion calorimetry as a function of consolidation temperature. Chapter 4.0 will cover in detail how the activation energy of the composite as a function of consolidation temperature was measured using a custom built ignition apparatus.

To compare the consolidation and the performance results from the sol-gel derived Ta-WO_3 composite, a commercially available WO_3 (crystalline) with macrometric Ta thermite composite was mixed. This commercially available thermite composite was exposed to the same consolidation parameters as the sol-gel derived and its performance was tested under the same conditions as the sol-gel derived composite.

Chapter 2

Synthesis, Small Scale Testing and Consolidation of Tantalum-Tungsten Oxide Thermite Composites

2.0 INTRODUCTION

The search for new energetic materials continues to be motivated by the desire to optimize performance and sensitivity. Energetic composites are of significant interest due to the wide range of material properties that can be tailored by controlling the chemical composition and the particle size of the fuel metal and oxidizer.

One of the exciting potential applications of energetic composites is as multifunctional energetic material (MFEM). MFEM's draw inspiration from natural systems and are energetic materials that in addition to providing stored chemical energy afford at least one other desired attribute that can be utilized in an engineered system. In many cases this second attribute is mechanical strength. Potential applications that may envision utilizing MFEMs are thermal batteries, micro-electro-mechanical systems, and anti-tamper devices [38] As mentioned, one of the critical the two functionalities afforded by MFEMs is mechanical strength. For a given material optimal mechanical strength is realized as that system approached theoretical maximum density. Therefore one of the aims of this study was to investigate processing conditions that gave high densities.

Rates and mechanisms for fully dense self-propagating high temperature synthesis (SHS) thermite reactions have only been available from studies of a limited number of materials [14, 39]. In the present study we have investigated the system where Ta is the fuel metal and WO_3 is the oxidizer. Ta-WO_3 is a particularly interesting system because of its high theoretical density (9.85 $g \cdot cm^{-3}$). The stoichiometric thermite reaction for the Ta-WO_3 energetic composite can be described by the following equation:

$$6\ Ta + 5\ WO_3 \rightarrow 3\ Ta_2O_5 + 5\ W \qquad 2\text{-}1$$

The enthalpy of the above reaction is -174.879 $kJ \cdot mol^{-1}$, giving an adiabatic combustion temperature of 2181°C. The enthalpy of Eq. (2.1) was determined using the HSC Chemistry Version 4.0 software [40].

We have developed sol-gel processes that enable the production of a wide range of metal oxides and their precursors [41]. The process takes advantage of recent progress in the use of organic proton scavenging agents to produce metal oxide precursors. The precursors can then be processed into aerogels, xerogels, or nanopowders of the desired materials. The method is especially versatile as it enables the facile incorporation of additional phases into the composite [42]. This approach has been used successfully to prepare energetic nanocomposite materials [8, 41]. Using these techniques allows for the tailoring of the product morphology, crystallinity, and even the production of nanocomposite powders [43-45]. The sol-gel technique makes it possible to

tailor the particle size of the fuel metal and oxidizer independently and therefore the energy delivery rate (finer composites lead to higher power generation) [46].

The goal of this study was to synthesize nanostructured, amorphous WO_3 with immobilized Ta metal particles using sol-gel techniques and to consolidate the Ta-WO_3 energetic composite to near theoretical density without significant reaction to ensure complete retention of the chemical energy. To achieve densification without reaction, it is necessary to use accelerated consolidation techniques. One such technique is spark plasma sintering (SPS). The process combines the application of pulsed DC current with uniaxial pressure. Its advantages stem from a combination of factors including high heating rate (up to about 2000°C·min^{-1}), high pressure (up to about 1 GPa), and electromigration [36]. The high pressure is obtained in a modification of die design, as has been reported previously [37]. We utilized this modified SPS technique in our study, which we will refer to as High Pressure Spark Plasma Sintering (HPSPS).

2.1 EXPERIMENTAL METHODS

2.1.1 Synthesis of WO_3 sol-gel and formulation of Ta - WO_3 composites

The tungsten salt used in this study was $WOCl_4$ (F.W. = 342 g·mol^{-1}; 98% pure from Sigma-Aldrich, Milwaukee, WI). The epoxide used as a gelation agent was 3,3,-dimethyloxetane (DMO) obtained from Sigma-Aldrich and reported to be 98% pure. The solvents utilized were 200 proof ethanol (Pharmco-AAPER, Brookfield, CT), cyclohexane (ACS reagent ≥ 99% purity from Sigma-Aldrich, Milwaukee, WI), de-ionized and distilled water.

A typical gel synthesis experiment involves the following steps: 14.76 g (43.5 mmol) of $WOCl_4$ was dissolved in 125 mL of an ethanol/H_2O solution with a 95/5 vol % composition. Dissolution of the tungsten salt results in a solution that was slightly turbid. This solution was subsequently filtered through a Buchner funnel lined with filter paper to give a clear colorless solution. Then 20 g (235 mmol) of DMO was added (epoxide/metal ion ratio of 5.4) to the $WOCl_4$ solution while stirring. With the use of epoxides for this gelation in some cases significant heat generation is realized, which in some cases may lead to a flash boil of the synthesis solution. The cautious addition of the epoxide to the metal salt solution is recommended in a well-ventilated space [47]. In all cases, a rigid white gel formed within 5 min after addition of the DMO. Formulation of the Ta-WO_3 composites followed a procedure identical to that described above with the exception that 9.2 g (52.2 mmol) of capacitor grade Ta metal (H.C. Starck; average particle size 5 μm and 99.99% pure) was added. For the composite the mixture was stirred rapidly, with a Teflon-coated stir bar on a magnetic stir plate,

to ensure uniform distribution of the Ta fuel metal throughout the matrix, until gelation occurred.

For comparison purposes, as-received commercial WO_3 (99.998% pure from Sigma-Aldrich, Milwaukee, WI) was purchase to distinguish any consolidation differences with the sol-gel prepared WO_3.

2.1.2 Processing of metal oxide gels

The wet gels and composite gels were covered and allowed to age for at least 24 h under ambient conditions. After that they were immersed in a bath of absolute ethanol where they were washed for ~3 days. The solvent was changed in the bath 1-2 times a day during this wash process. This process was necessary to wash out the organic byproducts of the DMO used in the synthesis. The wet gels were subsequently washed with cyclohexane for ~2 days, changing the solvent bath 1-2 times per day. The cyclohexane was decanted off and the wet gel dried at ambient temperature in a fume hood. After air drying the resulting WO_3 gel and composite gels were dried at 110°C under dynamic vacuum for 24 h. This preparation led to the synthesis of 10 g of WO_3 sol-gel material. Figure 3 shows a TEM image of the as-synthesized sol-gel WO_3. It can be observed that the particle size is approximately 10 nm. The surface area of the sol-gel derived WO_3 was measured to be 141 $m^2 \cdot g^{-1}$ by the BET method [48].

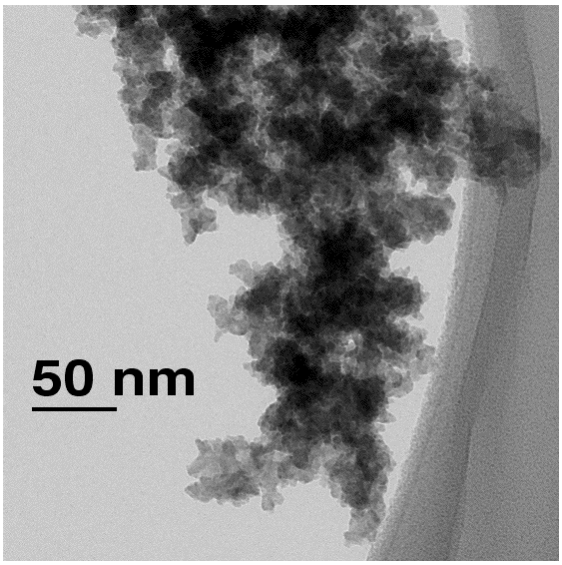

Figure 3: A TEM image of the as-dried WO_3.

2.1.3 Initial Ta - WO_3 powder formulations

Due to processing and handling safety concerns, the adiabatic temperature of several highly fuel deficient, (i.e., sub-stoichiometric with respect to Ta) energetic composite powders was calculated using the HSC Chemistry Version 4.0 software [40]. We calculated the adiabatic reaction temperatures while varying the stoichiometric Ta content. An example of sub-stoichiometric reaction containing 10 mol % of the stoichiometric quantity of Ta is

$$0.6\ Ta + 5\ WO_3 \rightarrow 0.3\ Ta_2O_5 + 0.5\ W + 4.5\ WO_3 \qquad 2\text{-}2$$

The excess WO_3 in the above equation acts as a diluent leading to lower adiabatic reaction temperature. As stated above, the adiabatic combustion temperature for Eq (2-1) is 2181°C and with this dilution, the adiabatic

temperature for Eq (2-2) is 450°C. Table 1 shows the calculated adiabatic reaction temperatures while varying the stoichiometric Ta content.

Table 1: Adiabatic reaction temperature of the Ta-WO_3 thermite reaction with varying Ta content.

Ta [% of stoichiometric value]	T_{ad} [°C]
100	**2181**
50	**1472**
40	**1394**
30	**1106**
20	**788**
10	**450**

2.1.4 Characterization of WO_3 and Ta-WO_3 powders

Morphology and composition of the energetic composites were examined on a Hitachi S4500 field emission scanning electron microscope (SEM) operated at 10 kV in backscattered-electron mode. The Ta-WO_3 energetic composite was embedded in epoxy and polished using traditional polishing techniques for cross-section examination. The phase composition was determined for the as-received commercial WO_3, sol-gel prepared WO_3 and the Ta-WO_3 composite by X-ray diffraction (XRD). The XRD was performed on a Scintag PAD V powder diffractometer operated at 45 kV and 35mA using Cu $K_{\alpha 1}$ radiation (λ = 1.54056

Å). A JEOL transmission electron microscope (TEM) was used to determine the morphology and particle size of the WO_3.

2.1.5 Consolidation by Spark Plasma Sintering

In this study the HPSPS method was used to consolidate the Ta - WO_3 energetic composite. As previously stated, the HPSPS process combines the application of uniaxial pressure and pulsed DC current to a sample die assembly. The resistance of the sample die assembly to the pulsed DC current provides Joule heating to the powder sample. The advantages of HPSPS over conventional hot-pressing techniques are that samples using the HPSPS can be consolidated at high heating rates (up to about 2000°C·min^{-1}) while applying relatively high pressures. The method is described in detail elsewhere [37], but essentially consists of a graphite die assembly as shown in Figure 4. This die design allows for pressures as high as 1 GPa although in this study the pressure did not exceed 300 MPa. Heating rates were varied from 100 to 500°C·min^{-1}. Consolidation temperatures ranged from 300 to 600°C. Once the sample reached the desired temperature, the sample was held at temperature for 5 min.

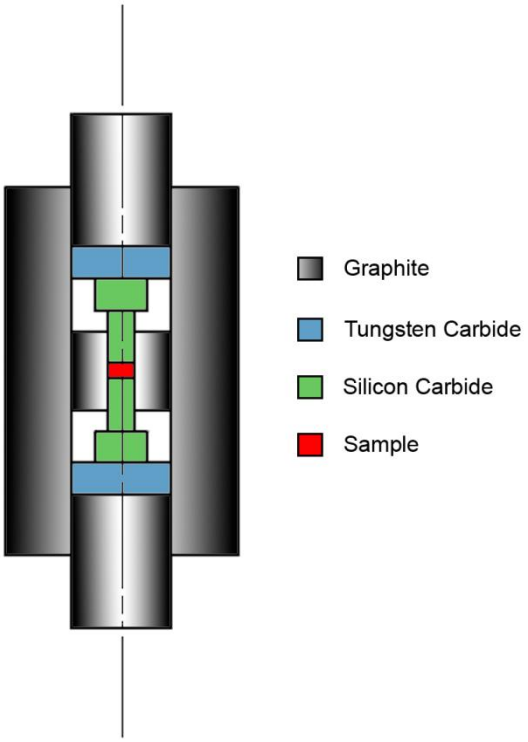

Figure 4: Schematic representation of high-pressure spark plasma sintering (HPSPS) die assembly

.

2.2 RESULTS AND DISCUSSION

2.2.1 WO_3 and Ta-WO_3 Powders

We have reported extensively on the use of organic epoxides as gelation agents for the sol-gel synthesis of a number of transition metal oxides from inorganic salt precursors [41]. A mechanistic study revealed that the epoxide acts as an irreversible proton scavenger that induces hydrolysis and condensation of metal ion species to form a sol [47]. These processes result in a slow and uniform pH increase throughout solution, which affords the uniform gel that is critical to the formation of a well dispersed composite. The structure and

substitution on the epoxide dictates its reactivity and thus affords some control over the rate of pH. In the case of tungsten (VI) the 1,2-epoxides, such as propylene oxide, react rapidly and result in precipitates instead of monolithic gels. By comparison, when 1,3-epoxides are used, the pH rise is slower presumably due to the lower reactivity, and in the case of tungsten (VI) salts leads to the formation of rigid monolithic gels.

We have utilized this synthetic approach to formulate nanostructured energetic materials [44,45]. The energetic ingredients and composites formulated using this methodology have unique reaction (combustion) characteristics that have been detailed elsewhere [7,8]. To briefly summarize the nanostructural evolution, the sol particles of WO_3 phase grow around and eventually encapsulate the solid suspended Ta particles to form a nanostructured energetic nanocomposite as the sol transforms to a gel. This process takes advantage of the viscosity increase of the sol-gel solution as it approaches its gel point. Once the gel forms the matrix is rigid and has effectively “frozen” Ta into place within the gel network. This process creates an energetic composite that consists of an intimate mixture of micron-sized crystalline Ta dispersed throughout a nano-network of amorphous tungsten (VI) oxide. Figure 5 is a backscattered-electron SEM image of as-dried Ta-WO_3 composite particles embedded in epoxy (dark gray). The lightest regions are Ta and the medium gray is amorphous tungsten (VI) oxide. Note that the tantalum particles are encapsulated by the tungsten oxide phase.

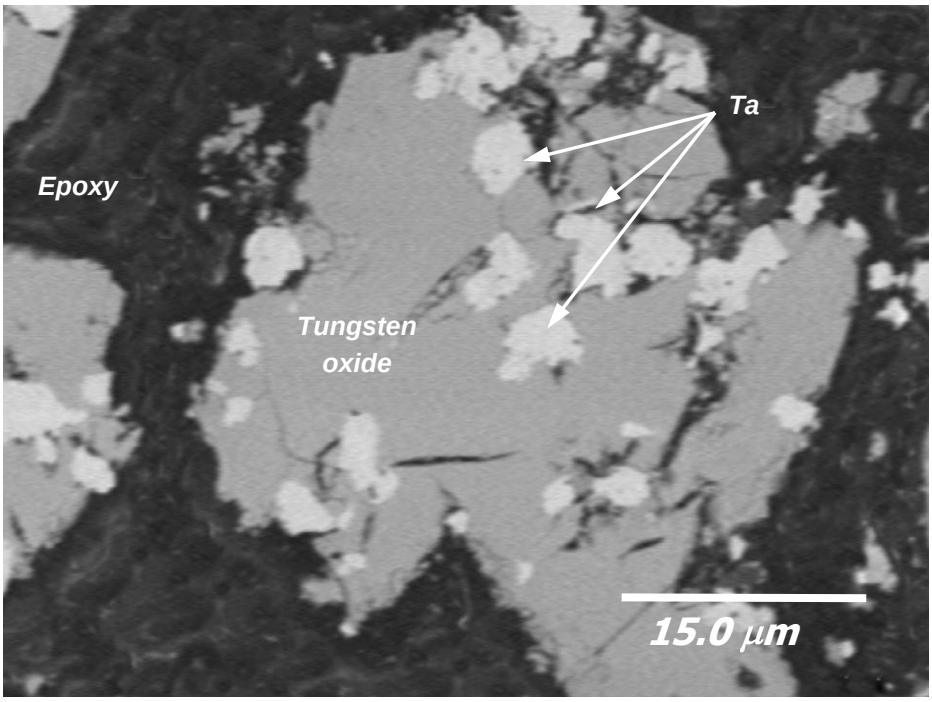

Figure 5: Backscattered-electron SEM image of as-dried Ta-WO_3 composite particles embedded in epoxy (dark gray). The lightest regions are Ta and the medium gray is amorphous tungsten (VI) oxide.

Figure 6 shows the XRD patterns for the as-received commercial WO_3 powder (Sigma-Aldrich, Milwaukee, WI),, the sol-gel prepared WO_3 and the Ta-WO_3 energetic composite. XRD analysis shows that the as-received commercial WO_3 powder has a crystalline structure. In contrast, the sol-gel prepared WO_3 shows two broad peaks which indicate that the powder has an amorphous structure. Additionally, the XRD pattern of the Ta-WO_3 energetic composite shows that the composite maintains the amorphous structure of the WO_3 while incorporating crystalline peaks from the Ta particles.

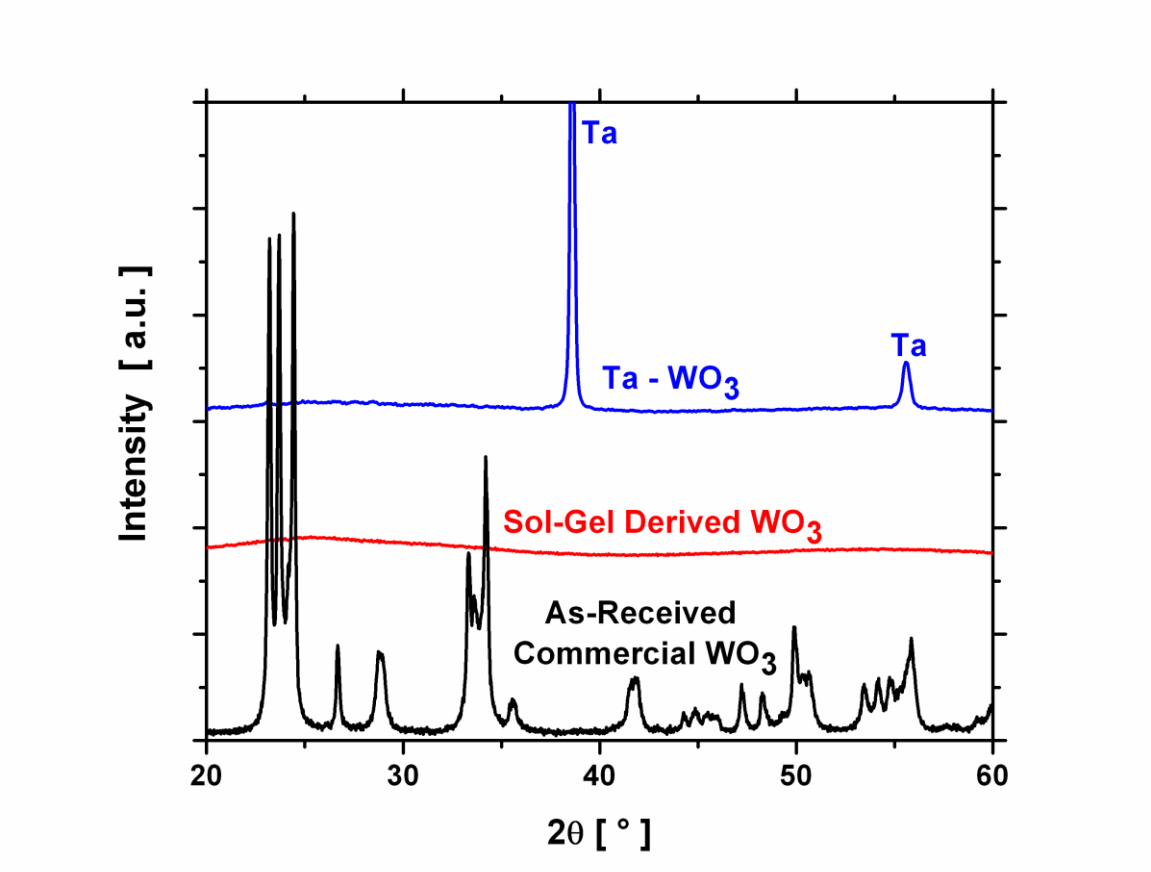

Figure 6: X-ray diffraction patterns from crystalline tungsten (VI) oxide (black), amorphous tungsten (VI) oxide (red) and energetic composite Ta-WO_3 powder (blue).

2.2.2 Small Scale Testing of Ta-WO_3 powder mixtures

Since the Ta - WO_3 composite mixture has a potential for large exothermic reaction and an adiabatic reaction temperature sufficiently high to self-sustain the reaction, we investigated the sensitivity of the composite by prescribed tests. These tests are designed to determine the sensitivity of the composite to friction, spark, and impact stimuli.

The response of composite formulations to friction was evaluated using a Bundesanstalt für Materialprufüngen (BAM) friction-testing machine manufactured by Julius Peters Company in Berlin, Germany [49]. This test provides critical information for safe material handling and processing. The tester utilizes a fixed porcelain pin and a movable porcelain plate that performs a reciprocating motion. Weights from 0.5 to 36 kg were attached to a torsion arm which allows for the applied force to be varied. The measure of frictional sensitivity of a material is based upon the largest pin load at which one ignition occurs in ten trials. The Ta-WO_3 composite was found to have zero events out of ten trials with the 36 kg weight on the torsion arm. Figure 7 shows a schematic representation of the friction – testing apparatus.

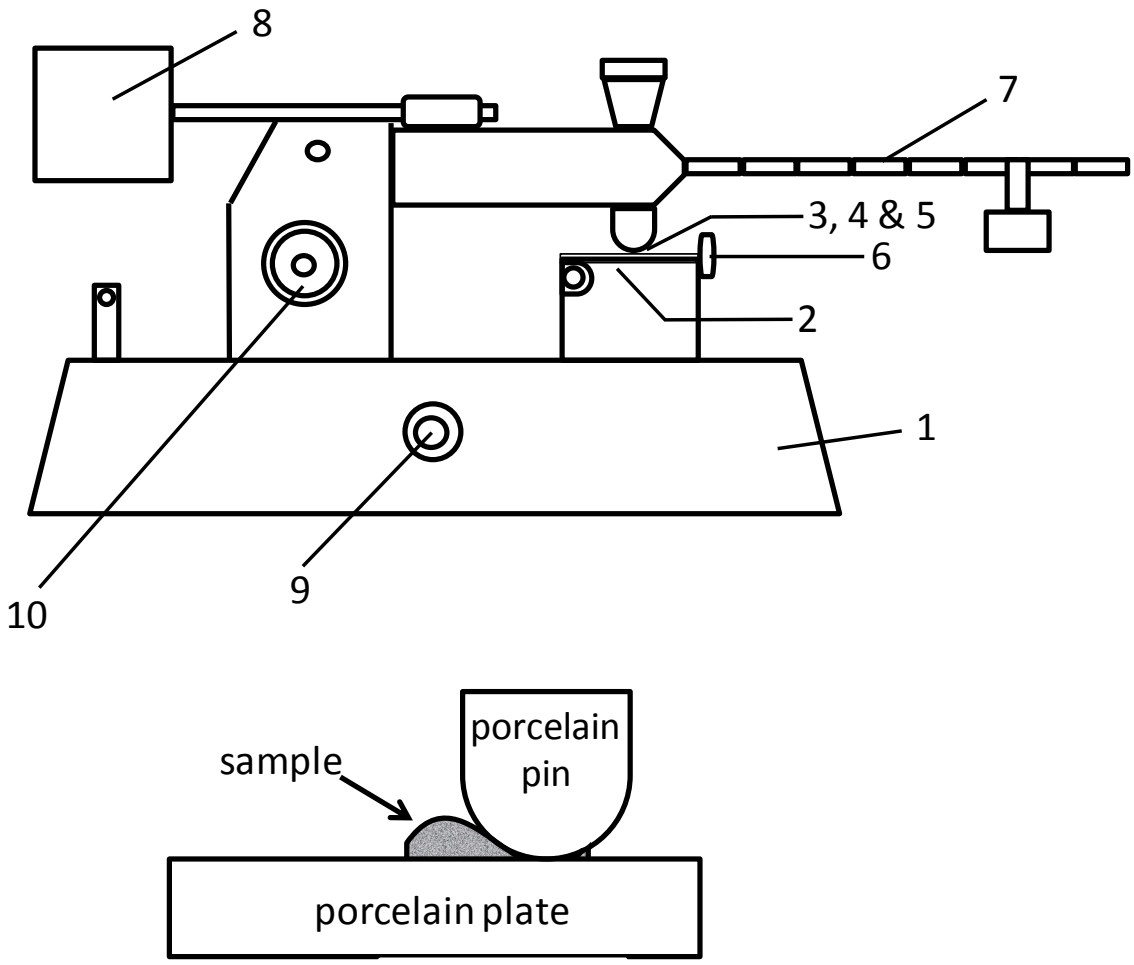

Figure 7: Side and top views of large BAM friction apparatus with load weight for determination of friction sensitivity of secondary explosives. Labeled are: 1) Steel base, 2) Movable carriage, 3) Porcelain plate clamped to carriage, 4) Fixed porcelain pin, 5) Sample on plate, 6) Adjusting rod, 7) Loading arm, 8) Counter weight, 9) Actuating switch, 10) Handle for setting the carriage at the starting position, 11) Electric motor connection.

The sensitivity of energetic composites toward electrostatic discharge was measured using a modified Electrical Instrument Services electrostatic discharge tester [50]. The instrument consists of three parts: the capacitor bank, a charging system and the discharging system. The capacitor bank has a range of

capacitance from 50 to 20,000 pF. The voltage range is up to 10,000 V and energy output up to 2 J. To perform the electrostatic measurement, a 35 mg portion of energetic composite powder was loaded into a metal stub with Teflon washer seated on top. The metal stub with the Teflon washer is then covered with 1 mm thick Mylar tape to keep the energetic composite powder from dispersing out of the metal stub. A spark discharge of variable energy is sent from an electrode tip to the sample. The sensitivity is defined as the highest energy setting at which no ignition occurs in ten consecutive trials. The lowest energy setting for this instrument is 0.04 J and the highest 1 J [50]. None of the ten powdered samples of Ta-WO_3 reacted at the highest energy input setting of 1 J. Figure 8 shows a schematic representation of the spark sensitive apparatus.

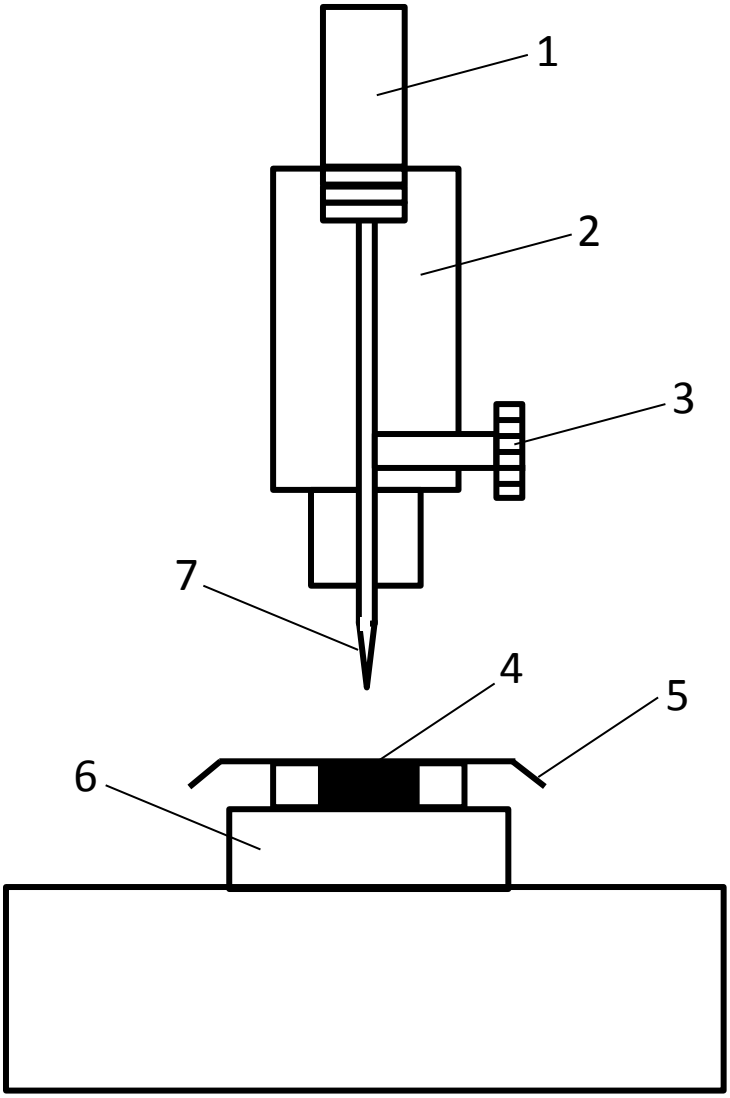

Figure 8: Schematic representation of the spark sensitive apparatus: 1) Brass shaft, 2) Brass holder, 3) Set screw, 4) Sample, 5) Mylar tape, 6) Witness steel block and 7) Phonograph Needle.

The impact sensitivity of energetic composites was evaluated with a drop hammer machine [51]. The drop hammer test is a quick and safe single way of determining the overall safety without using much sample. This is the best known way to evaluate impact sensitivity. To briefly discuss the process, a 2.5 kg weight is dropped from a given height on a tower towards a small amount (35

mg) of energetic composite material. Test results are reported as DH_{50}, a value that represents the height in centimeters at which the probability of reaction is 50% [51]. Samples of energetic composite were placed on a piece of carborundum paper sitting on a steel anvil. The weight is then dropped on the energetic composite. Visual events that constitute a reaction are any evidence of spark, flame, or report on impact. The operator made visual evaluations for ignition events**.** The Ta-WO_3 composite powder had zero ignitions out of fifteen trials at the highest drop height setting of 177 cm. Thus, the impact sensitivity of the composite was off scale for the instrument and therefore is quite insensitive to that stimulus. Figure 9 shows a schematic representation of the spark sensitive apparatus.

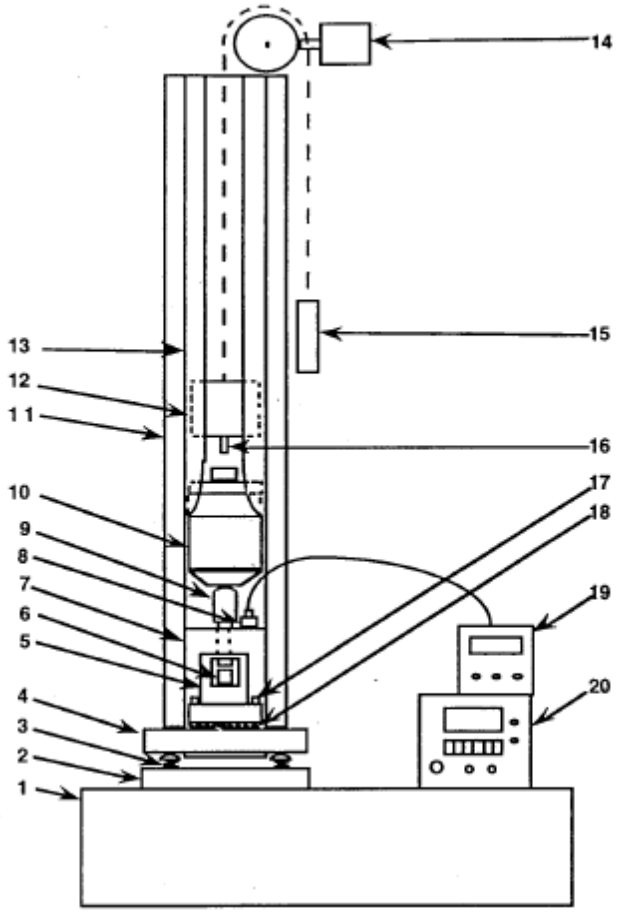

Figure 9: Components of the drop-hammer machine: 1) massive (top 3’ x 1’ x 3’, base 3’ x 2’ x 2’6”) concrete table, 2) 14” x 14” x 4” steel plate, bolted to table, 3) 4 adjuster (leveling) screws to bring drop weight into plumb, 4) a second 14” x 14” x 4” steel plate, 5) tool holder for lower anvil and striker, 6) lower anvil, 7) containment box, 8) microphone, 9) upper anvil or striker, 10) 2.5 drop weight, 11) support rails for guide tube, 12) drop mechanism, 13) guide tube, 14) height adjustment motor, 15) balance weight for drop weight, 16) “ball-lock” pin which holds/releases drop weight, 17) eight 3/8-16 socket head cap screws to hold tool assembly and screen down, 18) 16-mesh SS wire screen to reduce rebound, 19) voltmeter for microphone and 20) height control.

The sensitivity testing indicates that the composite material is insensitive to spark, friction, and impact stimulus. These results led us to conclude that the composite would be a good candidate for consolidation at elevated temperatures.

2.2.3 Consolidation of WO_3 powders

Initial consolidation studies were performed on sol-gel prepared tungsten oxide instead of the Ta-WO_3 energetic composite powders. This allows exploration of consolidation parameters necessary for the matrix material without concern for a thermite reaction occurring. As described in the experimental methods section, the tungsten oxide was consolidated by HPSPS using a range of consolidation temperatures from 300 to 600°C and pressures from 150 to 300 MPa. The displacement profile from an HPSPS experiment performed at 300 MPa and 600°C can be seen in Figure 10. Note that densification begins as low as 150°C and ends abruptly at ~375°C, such an abrupt halt is possibly indicative of crystallization. This sample resulted in a density of 6.75 $g \cdot cm^{-3}$, or 94.3% of the theoretical density of WO_3. For comparison, as-received commercial WO_3 powder sintered at 600°C and 300 MPa, only reached 5.32 $g \cdot cm^{-3}$ (74.3%). In contrast to the sol-gel prepared WO_3, the corresponding displacement and displacement rate data for the commercial WO_3 powder showed only negligible densification. This is indicative of an alternative densification method occurring in sol-gel prepared powders compared to crystalline commercial powder. We propose that this mechanism is likely viscous flow due the abrupt halt to displacement at 375°C which corresponds with XRD confirmed crystallization of the powder after heat treatment to 400°C. This is additionally confirmed by the lack of viscous flow in the already crystalline commercial powder. It appears that the amorphous nature of the WO_3 can allow densification of this composite by viscous flow at relatively mild consolidation conditions which enable densification

of energetic composites without significant pre-reaction. The low temperature consolidation of sol-gel prepared WO_3 leads to the possibility of consolidation of composite Ta-WO_3 powders to near full density without significant pre-reaction.

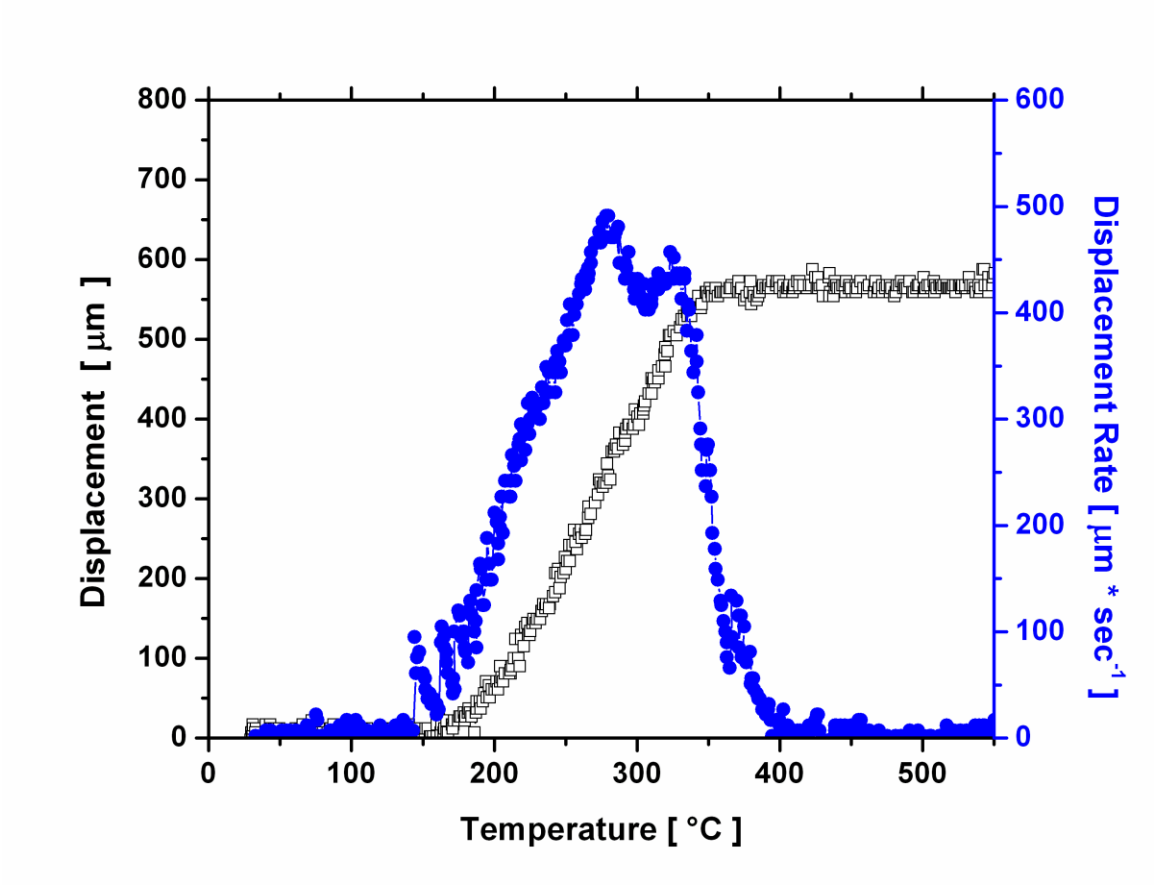

Figure 10: Displacement and displacement rate data for an HPSPS consolidation run at 300 MPa and 600°C.

2.2.4 Consolidation of Ta-WO_3 powders

After initial consolidation runs were achieved without ignition of the Ta-WO_3 energetic composite with sub-stoichiometric compositions, experiments continued with increasing Ta content until fully stoichiometric Ta-WO_3 thermites

were made. Figure 11 shows the density as a function of Ta content for samples consolidated at 500°C and 300 MPa. The highest achieved density of as-processed powders was 8.56 g·cm^{-3} (87%), but when powders were dried overnight 150°C to remove adsorbed water and consolidated under the same conditions, the maximum density increased to 9.17 g·cm^{-3} (93.3%) as depicted by the red triangle in Figure 11. This is due to the evolution of water vapor during the rapid consolidation of the as-processed powders leading to internal gas pressure in the pores and thus inhibited densification compared to the dried powders.

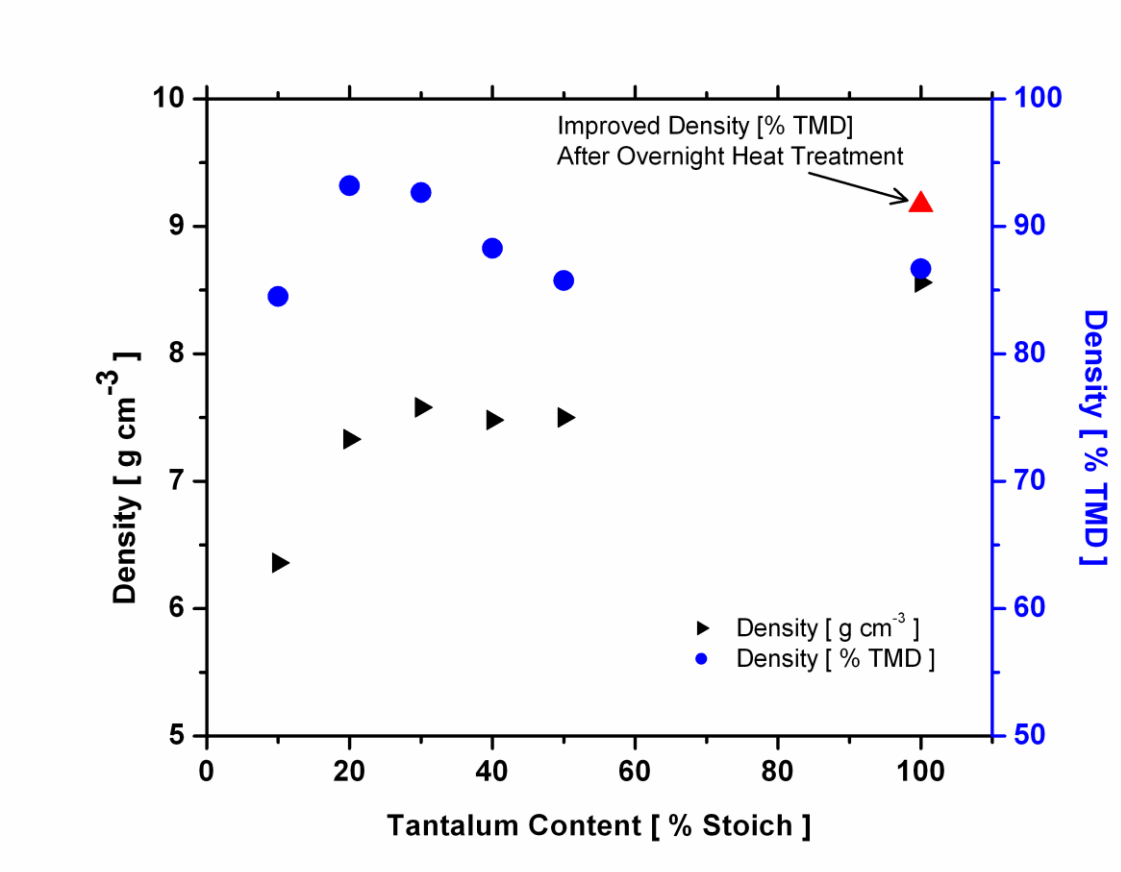

Figure 11: Density of Ta - WO_3 samples as a function of Ta content. All sample consolidated at 500°C and 300 MPa for 5 minutes.

2.2.5 Energy Release of Consolidated Ta-WO_3 pellet

In addition to the desired goal of consolidating the Ta-WO_3 energetic composite powder to high relative densities, the requirement that the consolidated samples retain a large fraction of their stored energy is imperative. Figure 12 shows a thermogram of a fully stoichiometric Ta-WO_3 sample consolidated to 85% relative density by HPSPS. The thermogram was obtained by securing the sample directly to a thermocouple and inserting the assembly into a furnace preheated to 1000°C. It can be observed that the there is a sharp temperature increase starting around 650°C which is indicative of the ignition temperature of the sample. Following the ignition temperature, we observe a peak temperature of approximately 1100°C. The thermogram shows that the sample has stored energy after consolidation. The inset image in Figure 12 shows a similar sample that has been initiated by a small torch. Detailed experiments are in progress to accurately determine the ignition and peak temperatures along with energy output of consolidated samples as a function of density and degree of pre-reaction.

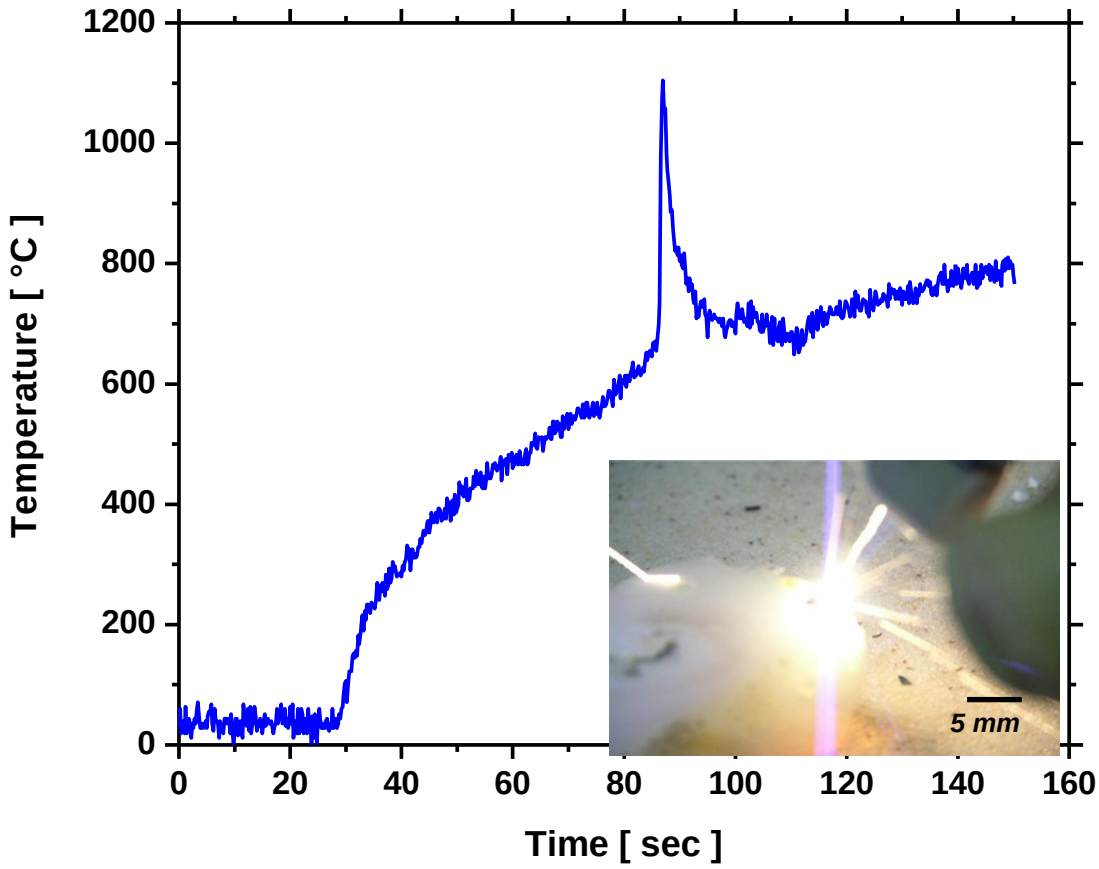

Figure 12: Plot of temperature versus time of a consolidated specimen during thermal initiation. Inset photo shows a sample initiated by open torch.

2.3 CONCLUSIONS

Ta-WO_3 energetic composite powders have been prepared by sol-gel synthesis with various amounts of Ta fuel and consolidated using the High Pressure Spark Plasma Sintering (HPSPS) technique. The uniqueness of the sol-gel synthesis is that instead of having separate loose powders of each constituent, we have a nanostructured WO_3 oxidizer in a gel form with the immobilized micron-size Ta fuel embedded in the gel. Such powder configuration permits for the constituents to be in intimate contact with one

another. In addition, the amorphous nature of the WO_3 oxidizer prior to consolidation allows for the densification of the energetic composite by viscous flow at relatively mild consolidation conditions. Furthermore, we have successfully consolidated the energetic composite powders to relative densities ranging from 84 - 93%. In addition, we have briefly shown that the consolidated samples retain stored energy, but have not quantified the energy output as a function of density.

LLNL-JRNL-410842

Chapter 3

Heat of Combustion of Tantalum-Tungsten Oxide Thermite Composites

3.0 INTRODUCTION

Nanostructured materials have been the focus of considerable interest due to their potential and demonstrated enhanced properties. An area where these materials have gained considerable interest is energetic composites. Energetic nano-composites are of significant interest due to the wide range of material properties that can be tailored by controlling their chemical and physical composition. It is understood that the reactants in energetic nano-composites have one or both reactants in the nanometric scale. Here we synthesized a sol-gel derived Ta-WO_3 energetic composite consisting of immobilized Ta particles inside a three dimensional nanometric network of amorphous tungsten oxide. This method produced an energetic composite in which the tantalum metal fuel is homogeneously distributed throughout the nanometric oxidizer. For comparison purposes, an as-received nano-crystalline commercially available tungsten oxide was mixed with tantalum metal particles using a mortar and pestle.

While considerable efforts have been aimed at understanding key properties such as reaction mechanisms, ignition sensitivity, energy release rates and activation energies of partially confined (< 50% Theoretical Maximum

Density samples) or loose powders, there appears to be a lack of studies on the heat of combustion of such metal-based energetic composites. For the most part, heat of combustion measurements are usually performed on carbon-based materials rather than metal-based materials. Moreover, studies on the effects of processing parameters have been performed in multilayer energetic materials [14], but not much has been done in powder energetic composites. Here we report results of an investigation on the heat of combustion of consolidated Ta-WO_3 composites as a function of consolidation temperature using the spark plasma sintering (SPS) technique.

3.1 EXPERIMENTAL METHODS

3.1.1 Synthesis of Ta-WO_3 Composites

Energetic composites of Ta-WO_3 were synthesized by two routes. In one we used a sol-gel (SG) derived method and in the second we mixed Ta and commercially available (CA) nanometric WO_3 powders. Due the lack of availability of nanometric tantalum, micrometric tantalum powder particles were used for both routes. A secondary-electron scanning electron microscope (SEM) image of the irregularly-shaped tantalum metal particles used in this work is presented in Figure 13 (a). The SG derived Ta-WO_3 mixture was made by dissolving 14.76 g (43.5 mmol) of $WOCl_4$ (F.W. = 339 g·mol^{-1}; 98% from Sigma-

Aldrich, Milwaukee, WI) in 125 mL of an ethanol/H_2O solution with a 95/5 vol % composition. After filtering the solution, 9.2 g (52.2 mmol) of capacitor grade Ta metal (H.C. Starck; average particle size 5 μm) was added to the filtered solution to make a composite mixture. While stirring the composite mixture with a Teflon-coated stir bar on a magnetic stir plate, to ensure uniform distribution of the Ta fuel metal throughout the matrix, 20 g (235 mmol) of 3,3,-dimethyloxetane (DMO) was added to the mixture. A gelation of a uniform composite occurred shortly thereafter. This method provides an energetic composite that consisted of immobilized micrometric tantalum into a three-dimensional nanostructured tungsten oxide gel with a 6:5 (Ta:WO_3) mole ratio. Further details on this method of synthesis of energetic composites can be found elsewhere [52]. The second preparation method consisted of mixing 48.2 wt% of the micrometric tantalum with 51.8 wt% of commercially available (CA) nanometric WO_3. The commercially available WO_3 was purchased from Sigma-Aldrich (Milwaukee, WI) and its average particle size was determined to be 48 nm by BET measurements [48]. Figure 13 (b) is an SEM image of the CA crystalline WO_3 powder. The mixing of the CA energetic composite was carried out by grinding in a standard ceramic mortar and pestle for approximately 5 min. Following the mixing, the powder mixture was placed in a glass vial and mixed further in a horizontal rolling mixer for another 5 min. A high magnification SEM image of the sol-gel derived amorphous WO_3 is presented in Figure 1 (c) and a high magnification SEM image of the commercially available crystalline WO_3 is shown in Figure 1 (d).

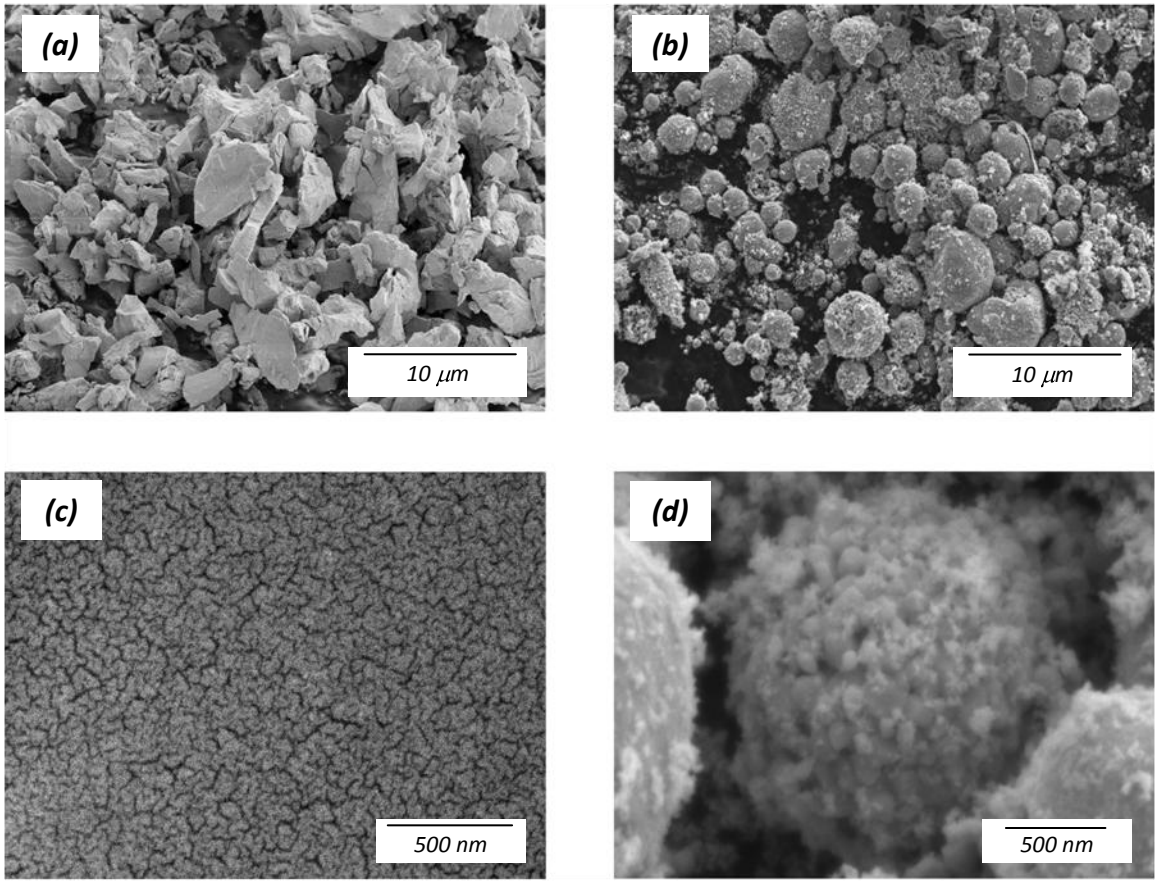

Figure 13: Secondary-electron SEM image of (a) irregularly-shaped micrometric tantalum powder, (b) commercially available crystalline tungsten oxide powder, (c) high magnification SEM image of sol-gel derived amorphous tungsten oxide powder and (d) high magnification SEM image of crystalline porous structure of commercially available tungsten oxide.

3.1.2 Materials Characterization

The chemical composition of the Ta-WO_3 sol-gel derived energetic composite was determined using the Inductively Coupled Plasma Atomic Emission Spectroscopy (ICP-AES) technique. Carbon and hydrogen residuals on the material were measured using a LECO CHN 2000 analyzer with a detection limit of 0.5 wt%. The morphology of the Ta fuel in the energetic

composite was examined using a Hitachi S4500 field emission scanning electron microscope (SEM) operated at 10 kV in secondary-electron mode. Cross-sectional images of the consolidated samples were taken in the SEM in backscattered-electron mode. Energy Dispersive Spectroscopy (EDS) measurements were performed using the Hitachi S4500 SEM mentioned above. The phase composition of each sample was determined by X-ray diffraction (XRD). The XRD was performed on a Scintag PAD V powder diffractometer operated at 45 kV and 35 mA using Cu $K_{\alpha 1}$ radiation (λ = 1.54056 Å).

3.1.3 Consolidation of Ta-WO_3 Composites

The consolidation of both the SG and the CA Ta-WO_3 energetic composites was performed using the high-pressure spark plasma sintering (HPSPS) method. Figure 14 shows a schematic representation of the HPSPS graphite die assembly used to produce our samples, please note that the internal components of the assembly are made up of tungsten carbide instead of the traditional tungsten carbide and silicon carbide combination presented in Section 2.1.5. Further details on the technique are found on [36, 37].

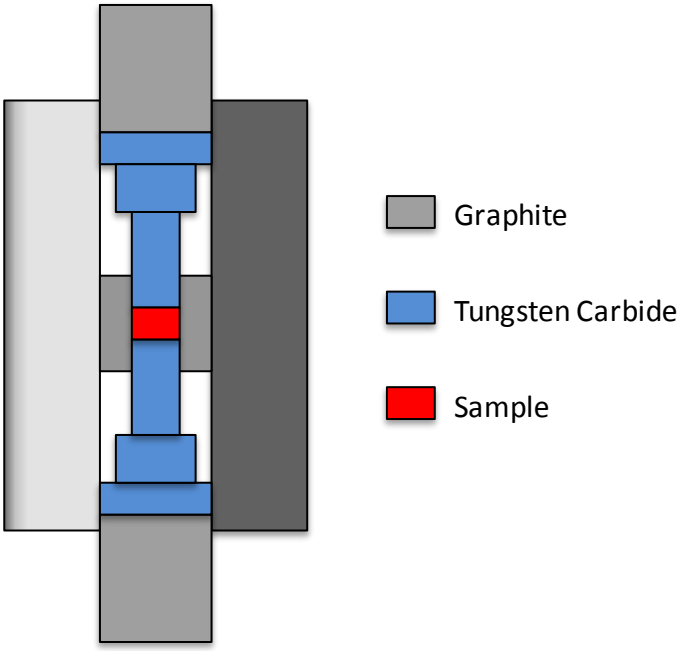

Figure 14: Schematic representation of high pressure spark plasma sintering (HPSPS) graphite die assembly.

Using 5 mm diameter graphite dies, the samples were consolidated at 25, 400 and 500°C. It should be noted that for the samples prepared at 25°C, the pulsed DC current in the HPSPS technique was not applied. The samples that were consolidated to 400 and 500°C were subjected to a pressure of 150 MPa and heated from room temperature to 200°C at approximately 50°C·min^{-1}. Then the samples were held at 200°C for 2 min in order to remove any residual solvents or physically adsorbed water. Following the 2-min hold, the pressure was increased to 300 MPa and the temperature increased to 400 or 500°C (at a rate of approximately 100°C·min^{-1}) and held for 3 min. The density of the resulting cylindrical pellets was determined by measuring the weight and dimensions of the pellet.

3.1.4 Heat of Combustion Measurements

The heat of combustion was measured using an oxygen bomb calorimeter (Parr 1261 Isoperibol Bomb Calorimeter, Parr Instruments Co., Moline, IL). The thermal mass of the bomb was determined prior to the calorimetric measurements. Calibration of the bomb was accomplished by combusting several certified benzoic acid samples of a known mass in a pure oxygen (99.99%) atmosphere. Once the thermal mass of the bomb was determined and the system calibrated, a Ta-WO_3 sample weighing approximately 0.2 g was place inside the bomb. A Chromel (chromium-nickel alloy) wire was connected to the two electrodes in the bomb and placed in contact with the sample for ignition. The bomb is then assembled and sealed. The bomb was then purged twice by pressurizing it to 2.0 MPa with oxygen. A third and final pressurization of the bomb was done at 2.0 MPa and the assembly was placed inside the calorimeter. Further details on the bomb calorimetry method are given elsewhere [53, 54]. The values reported here are averages of three separate measurements for each consolidation condition (25, 400 and 500°C) and from each energetic composite type (SG and CA). Table 2 reports the average composition of each composite.

Table 2: Chemical composition by weight percent of sol-gel derived (SG) and commercially available (CA) Ta-WO_3 energetic composite powders.

	Ta [%]	WO_3 [%]	Carbon [%]
Sol-Gel (SG)	45.7 ± 0.52	51.78 ± 0.66	2.52 ± 0.19
Commercially Available (CA)	46.5 ± 0.53	53.50 ± 1.95	< 0.5

3.2 RESULTS AND DISCUSSIONS

3.2.1 Consolidation of Energetic Composites

The SG and the CA energetic composites were consolidated as outlined in the experimental procedure. The theoretical maximum density (TMD) of the composites was calculated based on the results from the chemical analyses of each energetic composite. Table 2 shows the chemical composition for each composite. The theoretical maximum densities of the composites were calculated to be 8.90 $g \cdot cm^{-3}$ for the SG composite and 9.76 $g \cdot cm^{-3}$ for the CA composite. The difference in densities between the SG and CA composites is attributed to the fact that the SG composite contains 2.52 wt% carbon and the CHN analysis on the CA composite did not detect any measurable carbon. It is important to mention that TMD on the SG composite assumes that the carbon has a density of 2.09 $g \cdot cm^{-3}$ which is in the form of graphite. The idea of treating the carbon in the SG composite as a hydrocarbon was discarded since the CHN analysis did not detect any measurable hydrogen. Previous synthesis [47] of sol-gel derived composites have found polypropylene oxide (PPO) as a residual component in the material.

The dependence of the relative density of the composites on the sintering temperature is shown in Figure 15. For samples consolidated at 25°C, the average relative density for the SG composite was measured to be 56.41 ± 1.39% as compared to 62.32 ± 1.14% for the CA composite. A potential reason why the SG composite yields a lower density at 25°C than the CA composite

could be because the SG composite is a three-dimensional network powder with open porosity. In contrast, the reactants in the CA composite are made up of individual particles without any open porosity within each particle. Therefore, as the SG composite is consolidated at 25°C, the powder has to close the open porosity of the particles themselves and the gaps between each individual particle in the powder mixture. At sintering temperatures of 400 and 500°C the densities for both composites are within experimental uncertainties. Figure 15 shows that the average density for the SG composite is 81.30 ± 0.58% and is 74.54 ± 0.77% for the CA composite for samples consolidated at 400°C. For samples consolidated at 500°C, the average density for the SG composite was determined to be 84.42 ± 0.62% and was 77.90 ± 0.71% for the CA composite.

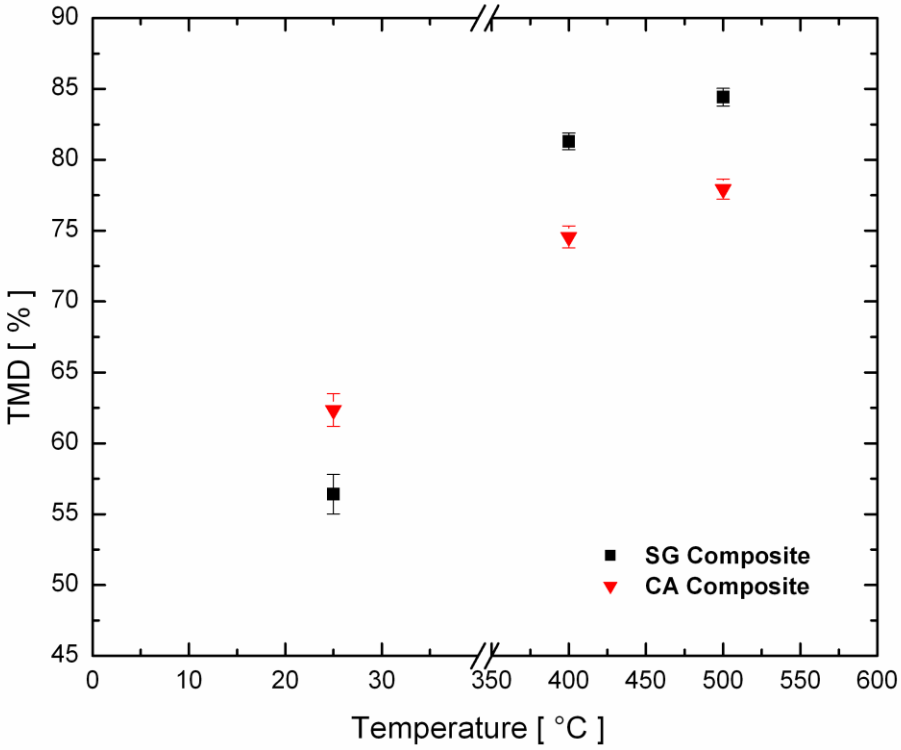

Figure 15: Theoretical Maximum Density vs consolidation temperature of both sol-gel (SG) derived and commercially available (CA) Ta-WO_3 energetic composites.

3.2.2 SEM Characterization of Energetic Composites

The morphologies of the CA and the SG derived Ta-WO_3 composites were investigated using the SEM technique in backscattered mode. Figure 16 shows the morphologies of the CA and the SG derived Ta-WO_3 composites consolidated to 400°C ((a) and (b)), respectively. The lighter gray particles correspond to the micrometric tantalum powder and the darker gray areas correspond to the tungsten oxide. For the most part, it can be observed that the

tantalum (lighter gray) is equally distribute in both composites consolidated at 400°C. Moreover, Figure 17 shows the morphologies of the CA and the SG derived Ta-WO_3 composites consolidated to 500°C ((a) and (b)), respectively. It can be observed that the tungsten oxide in the CA samples consolidated to 500°C preferentially aggregates in certain regions of the sample as observed by the elongated dark gray areas shown in Figure 17 (a).

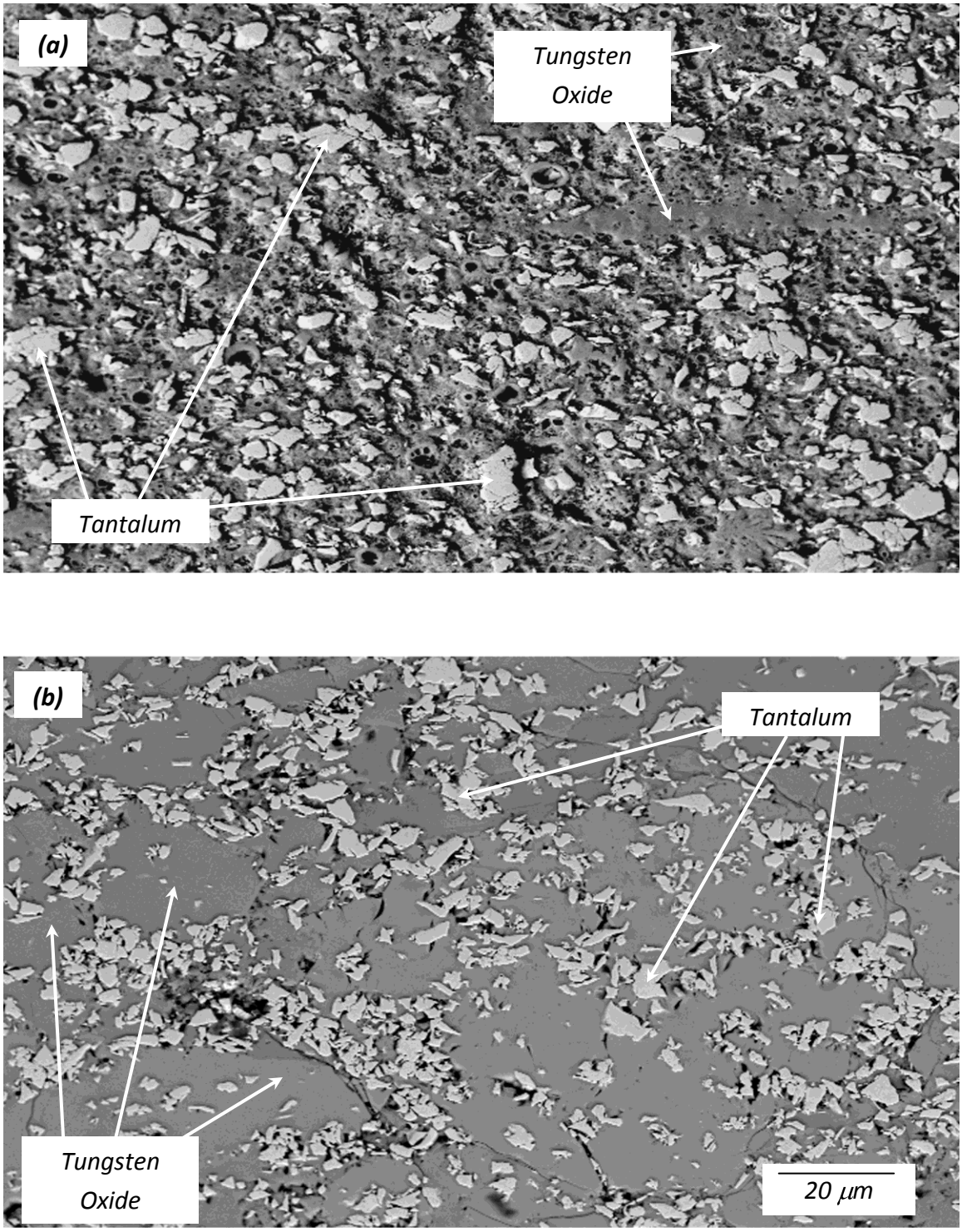

Figure 16: SEM images of (a) CA energetic composite consolidated to 400°C, (b) SG energetic composite consolidated to 400°C. The lighter gray corresponds to the tantalum powder and the medium gray to the tungsten oxide. The dark areas are voids in the consolidated samples. A pressure of 300 MPa was applied during the consolidation process to each sample using the HPSPS.

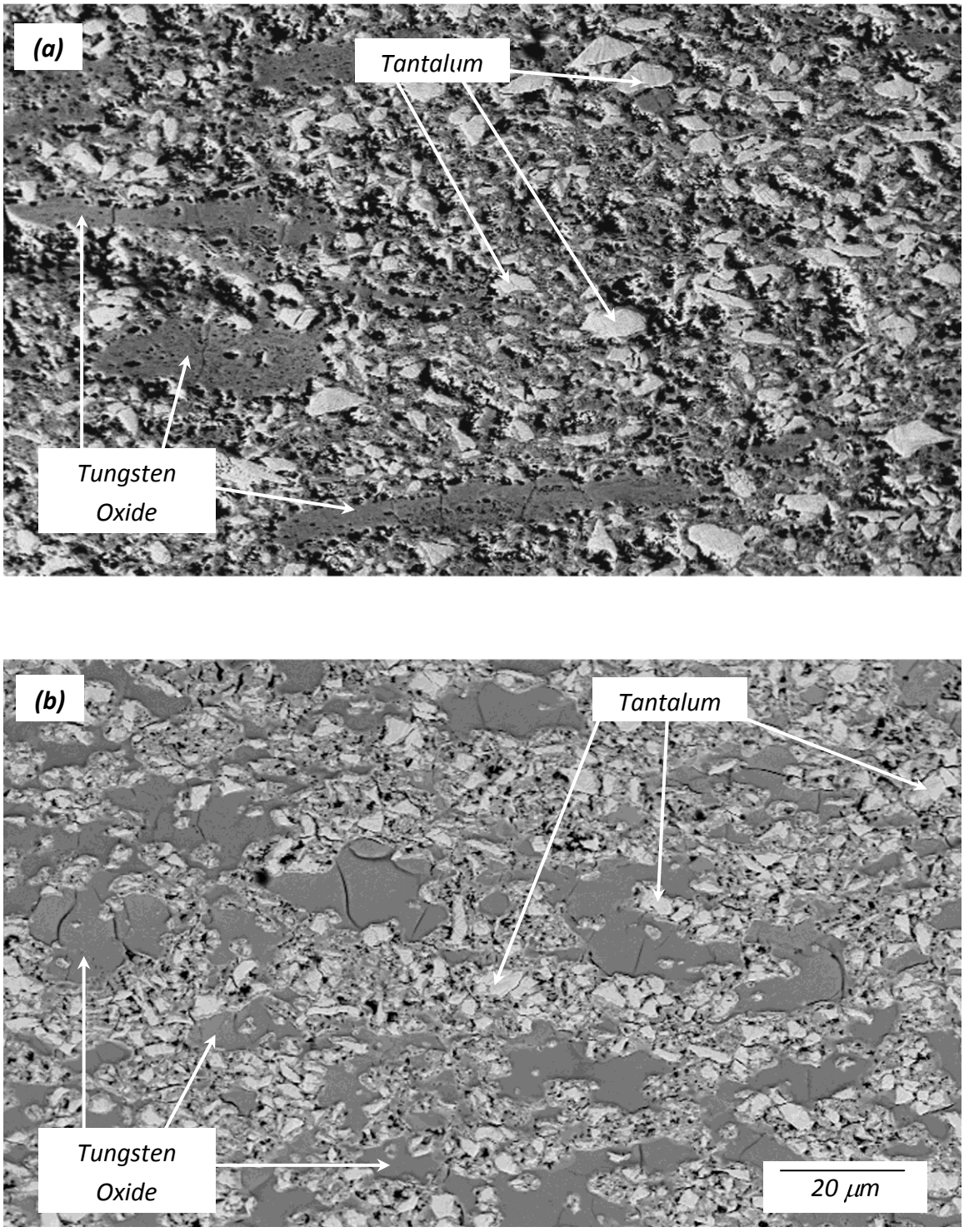

Figure 17: SEM images of (a) CA energetic composite consolidated to 500°C and (b) SG energetic composite consolidated to 500°C. The lighter gray corresponds to the tantalum powder and the medium gray to the tungsten oxide. The dark areas are voids in the consolidated samples. A pressure of 300 MPa was applied during the consolidation process to each sample using the HPSPS.

To explore the morphological effects of consolidation temperature on the pre-reaction of thermite composites, SEM images of both materials consolidated at 400 and 500°C were taken. Both materials showed similar morphologies, but for simplicity, only the images from the SG derived Ta-WO_3 will be presented as they show clear evidence of pre-reactions between the constituents. Figure 18 shows the morphology of the SG derived Ta-WO_3 consolidated to (a) 400°C and (b) 500°C.

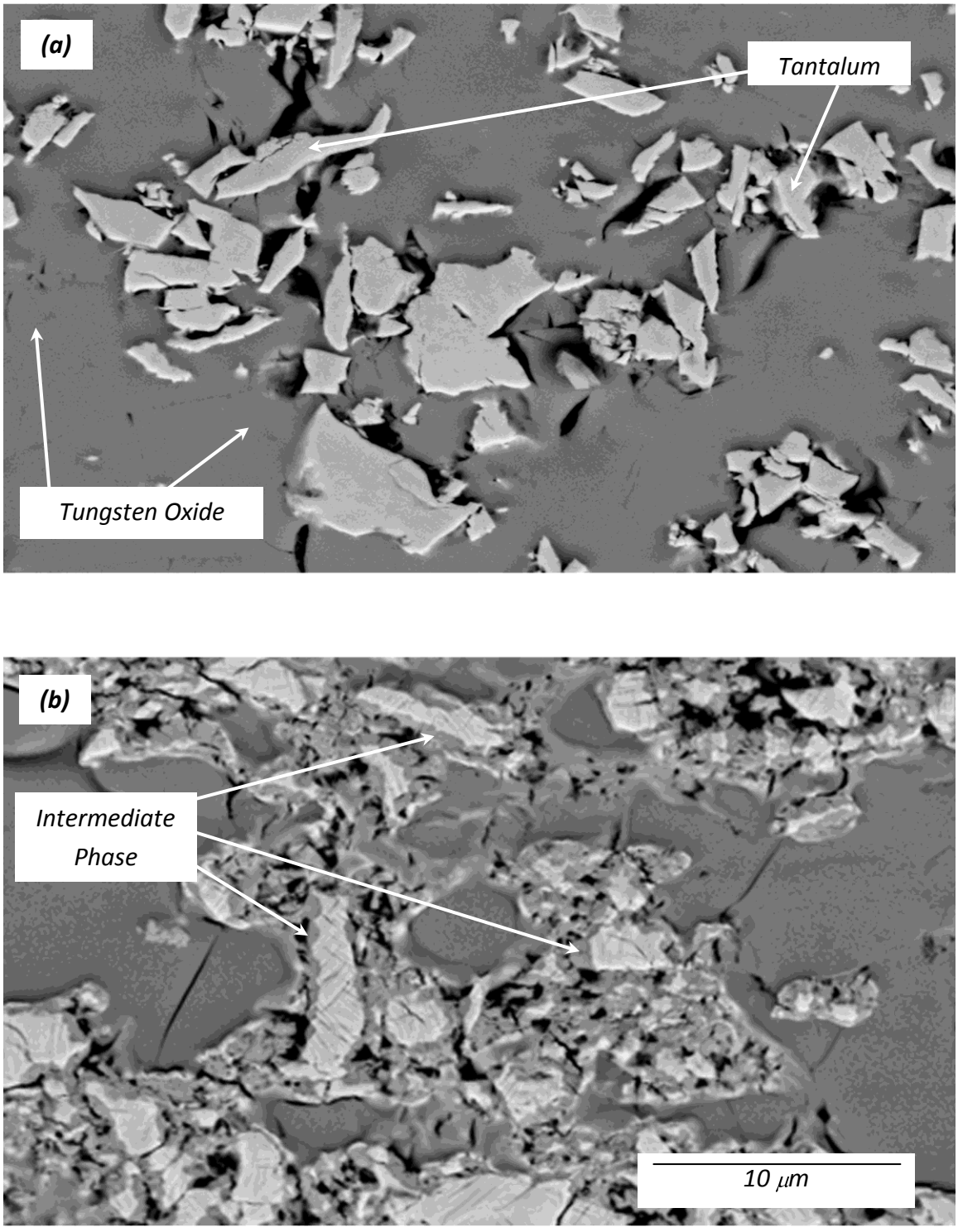

Figure 18: SEM images of (a) the SG energetic composite consolidated to 400°C and (b) SG energetic composite consolidated to 500°C. A pressure of 300 MPa was applied during the consolidation process to each sample using the HPSPS.

It can be observed that the sample consolidated to 400°C (Figure 18 (a)) does not show evidence of pre-reaction between the constituents since there is a distinct contrast difference in the interface between the tantalum (lighter gray) and the tungsten oxide (darker gray). In contrast, the sample consolidated to 500°C (Figure 18 (b)) shows evidence of pre-reaction as a new intermediate gray scale color interface between the tantalum and tungsten oxide has developed. Energy Dispersive Spectroscopy (EDS) measurements of the intermediate interface showed that the oxygen content is higher in this region than the oxygen content in the tantalum particle. In addition, the tungsten content in the intermediate gray area is lower than in the tungsten oxide region. This indicates that there has been an exchange of oxygen between the constituents, hence a pre-reaction.

3.2.3 Heat of Combustion

Using the HSC Chemistry Version 4.0 software [40], the theoretical heat of combustion for Eq (3-1) was calculated to be -2.734 $kJ \cdot g^{-1}$

$$6\ Ta + 5\ WO_3 + 7.5\ O_2(g) \rightarrow 3\ Ta_2O_5 + 5\ WO_3 \qquad 3\text{-}1$$

Eq (3-1) assumes that during the first step of the combustion reaction, the tungsten oxide gets reduced to tungsten metal and the tantalum metal gets oxidized. The excess oxygen in the bomb re-oxidizes the tungsten metal back to

its starting oxide state. In the process of the combustion reaction energy is released. The measured heats of combustion as a function of temperature of the SG-derived and the CA Ta-WO_3 composites are presented in Figure 19. As can be seen from the figure, the heat of combustion values for the SG composite consolidated at 25 and 400°C are higher than the theoretical value. For samples consolidated at 500°C, the measured heat of combustion is below the theoretical value. In comparison, the measured values for the CA composite are below the theoretical value for all conditions and decrease with increasing consolidation temperature.

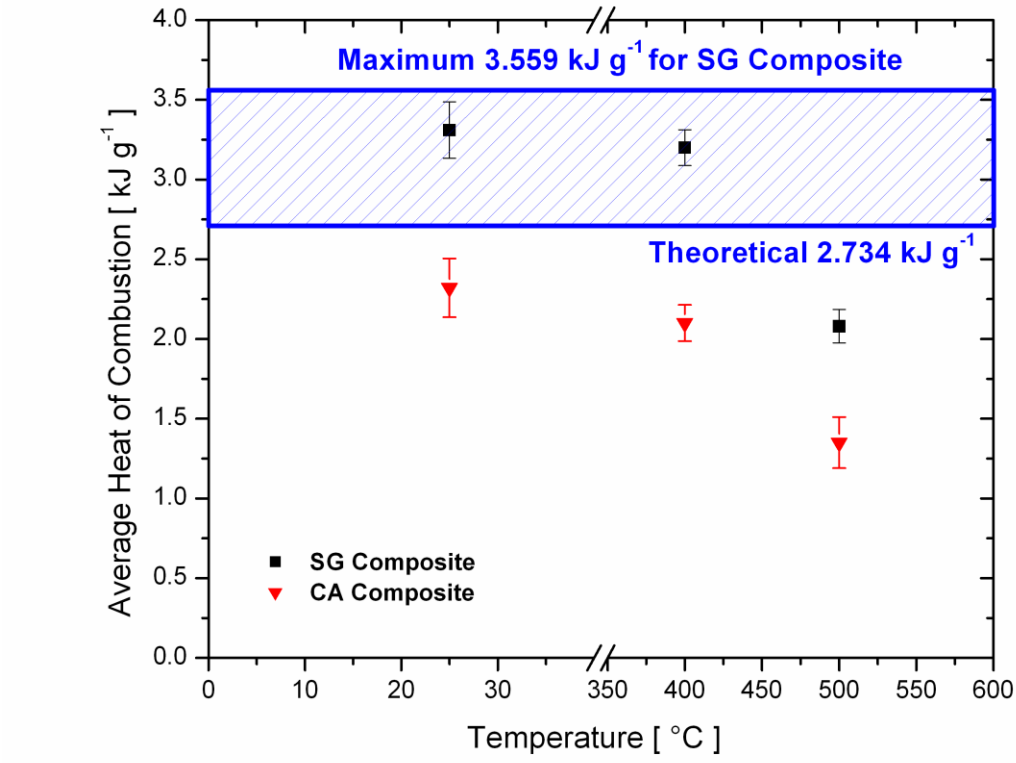

Figure 19: Average measured heat of combustion as a function of consolidation temperature of the SG and CA energetic composites.

Elemental analyses were performed on both the SG and CA energetic composites. Table 2 shows that the SG composite contains an average of 2.52 wt% carbon. The presence of this carbon is likely the cause of the observed higher heats of combustion than the theoretical value. The excess carbon originates from the synthesis of the SG composites. The measured heat of combustion of carbon (graphite) is reported to be -32.764 $kJ \cdot g^{-1}$ [55]. Assuming that the measured heat of combustion values for samples consolidated at 25 and 400°C are a result of the carbon present on the samples, the maximum heat of combustion value calculated from the Ta-WO_3 samples plus the contribution of the 2.5 wt% carbon in the composite is 3.559 $kJ \cdot g^{-1}$. Figure 19 shows that the measured heat of combustion values for the SG derived Ta-WO_3 composite samples are within the blue shaded area between the theoretical heat of combustion value and the maximum heat of combustion value. Therefore the assumption that the higher heat of combustion values are attributed by the carbon is appropriate. While calculating the difference in heat output between the SG and the CA composites, it was found that the SG composite generates about 30 to 35% higher heat output than its CA counterpart.

3.2.4 X-ray Diffraction Analysis

X-ray diffraction patterns of the SG and CA samples were obtained for each of the consolidated pellets at each temperature. Figure 20 shows the

diffraction patterns of pellets consolidated at 25°C for both the SG and the CA energetic composites. It can be observed that the SG derived composite is a mixture of crystalline Ta and amorphous WO_3. In contrast, Figure 20 shows that the CA diffraction pattern indicates the presence of crystalline Ta and WO_3.

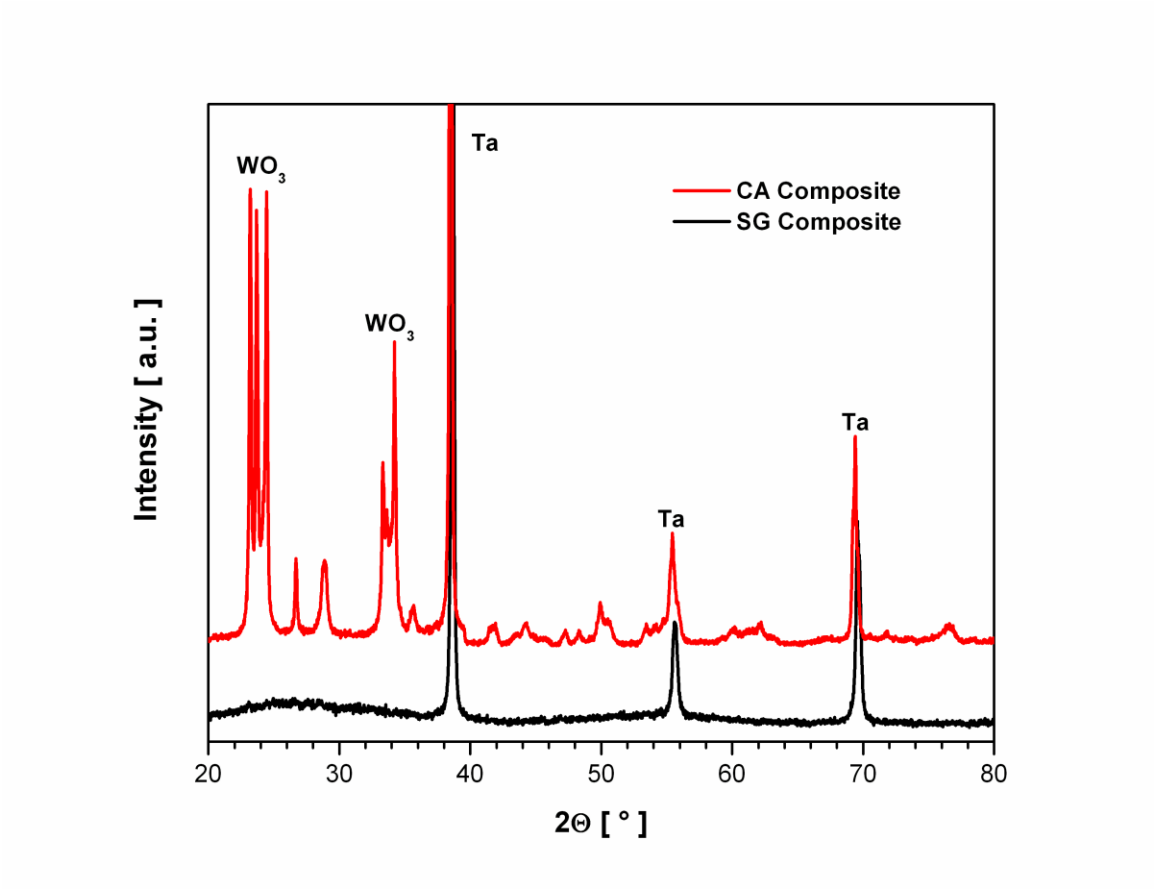

Figure 20: XRD of SG and CA energetic composite pellets consolidated using HPSPS to 300 MPa at 25°C.

As the consolidation temperature increases to 400°C, the Ta and the WO_3 begin to react in both the SG and the CA composite. Such reaction is indicated by the three high intensity peaks (labeled as peak 1, peak 2 and peak 3) next to the Ta peak located at 38.4° (2θ) as shown in Figure 21. All three peaks have

been identified as a Ta suboxide. The Ta suboxide that best fits these peaks is in the form of TaO_x as presented by Brauer, et. al [56]. In addition, two other crystallographic changes occurred while consolidating Ta-WO_3 at 400°C. The first change that can be observed is a decrease in the intensity of the WO_3 peaks in the CA composite, as can be seen by comparing Figure 20 and 7. The second crystallographic change is that the amorphous WO_3 present in the SG composite as shown in Figure 20, has started to crystallize and react with the Ta to form some complex tantalum tungsten oxide, tungsten oxide and tungsten suboxide as observed by the presence of several peaks that were not present in Figure 5.

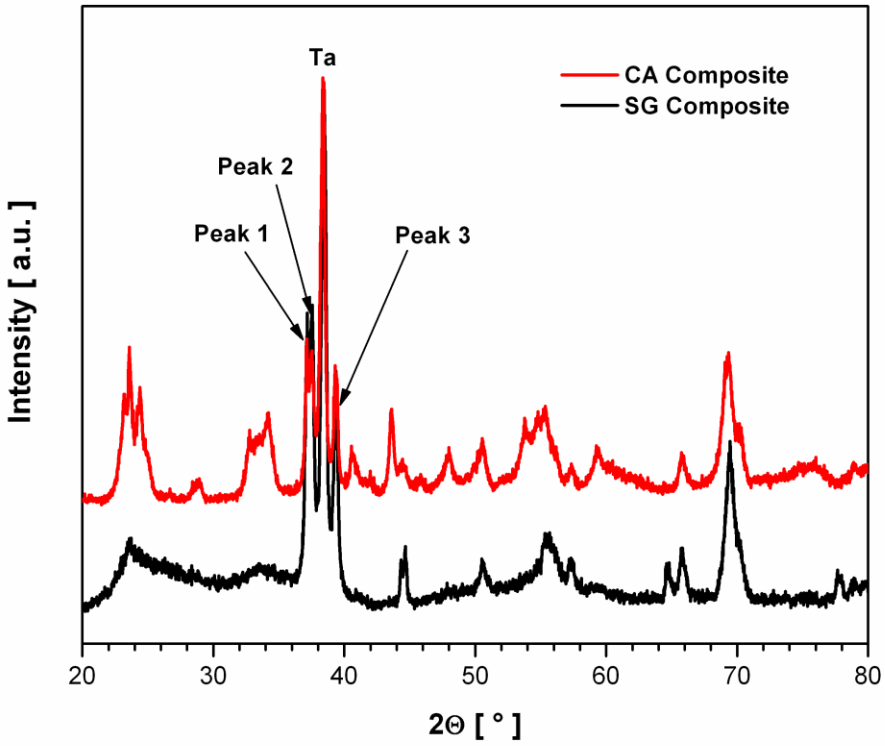

Figure 21: XRD of SG and CA energetic composite pellets consolidated using HPSPS to 300 MPa at 400°C.

Although it is difficult to properly identify these peaks, XRD analysis suggests that these peaks are from Ta_yO_x + WO_{3-x}, WO_3 and WO_{3-x}. Several studies have been perform on the oxidation of tantalum [56, 57] and oxidation of tungsten [58] and have reported that these metals undergo several phase transformations as a function of increasing temperature. The appearance of tantalum suboxide and tungsten suboxide peaks, the reduction in intensity of the WO_3 in the CA composite and the crystallization and reaction of the amorphous WO_3 with the Ta metal in the SG composite indicates that the Ta and WO_3 have begun to chemically react for samples consolidated to 400°C.

The x-ray diffraction patterns of the SG and the CA composites consolidated at 500°C are presented in Figure 22. At this temperature, the reaction between the Ta and the WO_3 has increased significantly (as can be seen by comparing Figure 20 to Figure 21). From the diffraction patterns it is apparent that Ta has reacted with the WO_3 to form Ta_2O_5, TaO, and W metal. For the SG energetic composite in Figure 22, it is seen that three of the most intense peaks, located at 2θ values of 22.98°, 28.52° and 36.96°, correspond to Ta_2O_5. Also it is noted that the intensity of the tantalum peak located at 2θ of about 38.4° has decreased significantly in comparison to Figure 20. A similar trend to the SG composite is seen for the CA composite as shown in Figure 20. The difference between the SG composite and the CA composite consolidated at 500°C is that the most intense peak in the CA composite is broad and can be indexed to TaO, WO_3 and W metal, instead of the Ta_2O_5 as in the case for the

SG composite. It is believed that since the CA composite does not incorporate immobilized Ta in the sol-gel matrix and instead is composed of individual fuel (Ta) and oxidizer (WO_3) particles, the reaction rate between the reactants is slower since the diffusion lengths are longer. The slower reaction rate due to longer diffusion lengths may explain the reason why we observe a strong TaO and W metal intermediate phase.

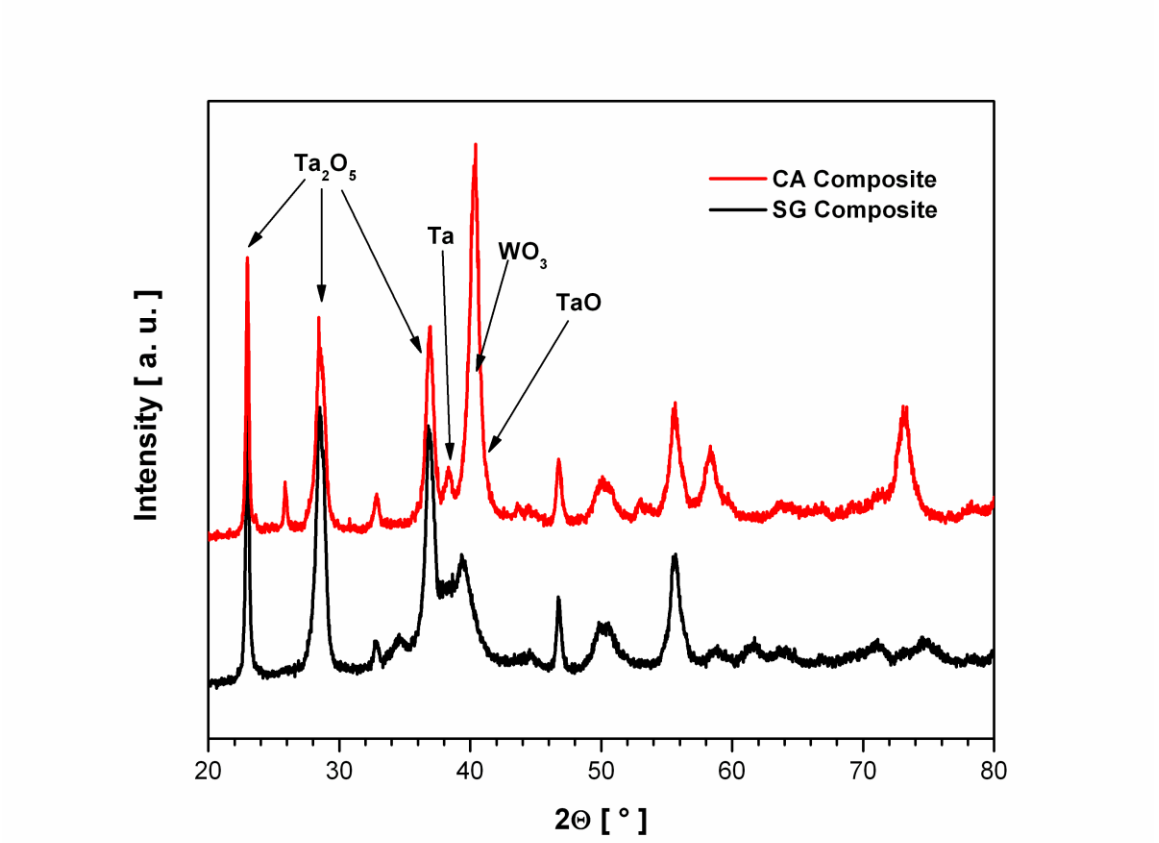

Figure 22: XRD of SG and CA energetic composite pellets consolidated using HPSPS to 300 MPa at 500°C.

It is likely that as the WO_3 is reduced, as shown in Eq (3-2), it liberates oxygen and it oxidizes the tantalum metal present in the Ta-WO_3 composite. The oxidation of tantalum metal yields two distinct tantalum oxide phases as shown in

Eqs (3-3) and (3-4). Hence, the reduction of tungsten oxide and the oxidation of tantalum in the Ta-WO_3 composite is a sequential process during the consolidating in HPSPS at 400 and 500°C:

$$WO_3 \rightarrow W + 1.5\ O_2\,(g) \qquad 3\text{-}2$$

$$2\ Ta + O_2\,(g) \rightarrow 2\ TaO \qquad 3\text{-}3$$

$$2\ Ta + 2.5\ O_2\,(g) \rightarrow Ta_2O_5 \qquad 3\text{-}4$$

XRD scans of the pellets consolidated using HPSPS at a pressure of 300 MPa and temperatures of 25, 400 and 500°C show that the amount of pre-reaction between the Ta and the WO_3 reactants in the energetic composite increases as a function of increasing consolidation temperature. A correlation can be found between the amount of pre-reaction of the constituents and the measured heat of combustion. Figure 19 shows that as the consolidation temperature increases the measured heat of combustion decreases. This can be attributed to fact that the pellets consolidated at 500°C experience higher degrees of pre-reaction in comparison to pellets consolidated at lower temperatures.

3.2.5 Characterization of Post-Combustion SG and CA Energetic Composites

During the post-combustion characterization of the energetic composites it was found that there was a distinct difference between the SG and CA composites. The remaining SG material was fragile and had a powder-like appearance. It took almost no effort to make into a powder for further analysis. In contrast, the CA composite was rigid, hard and had the shape of a small nugget. In order to make it into a powder, a significantly higher effort was required when compared to the SG composite.

The post-combustion phase composition of both energetic composites was investigated using the x-ray diffraction technique. Figure 23 shows post-combustion x-ray diffraction patterns from (a) SG energetic composite consolidated to 500°C and (b) CA energetic composite consolidated to 500°C. Analysis of the XRD pattern reveals that the remaining phase composition of the SG derived Ta-WO3 composite is best indexed to two complex tantalum-tungsten oxides ($3WO_3 \cdot Ta_2O_5$ and $Ta_{22}W_4O_{67}$) and tungsten oxide (WO_3). No apparent tungsten metal was identified from the XRD analysis. In contrast, post-combustion XRD analysis on the CA composite (Figure 23) shows evidence of tungsten metal as indicated by the peaks labeled as the W. The presence of tungsten metal on the remaining powder was verified by EDS measurements.

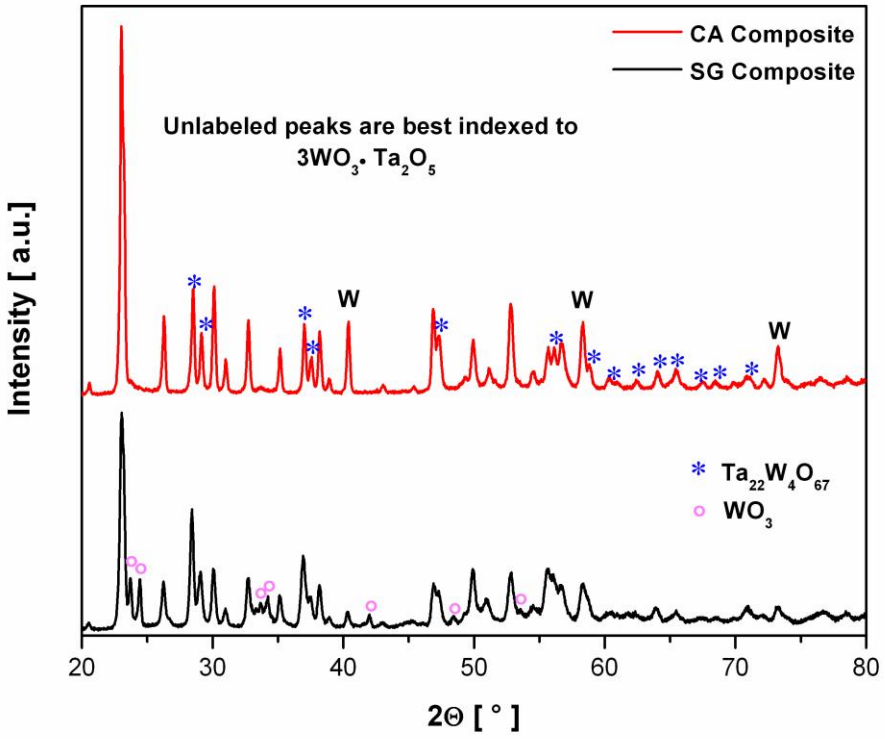

Figure 23: Post-combustion XRD patterns of the SG and CA energetic composite pellets consolidated to 500°C and 300 MPa using HPSPS. I still need to get the XRD pattern for the CA composite.

Figure 24 shows cross-sectional SEM images of the (a) SG and (b) CA post-combustion powders consolidated to 500°C. It can be observed that the morphologies are quite different, but most importantly, the SG composite does not show any evidence of tungsten metal whereas the CA powder shows tungsten metal particles as shown by the light gray spheres. The presence of tungsten metal on the CA powder indicates that the thermite reaction is an incomplete reaction as the excess oxygen in the bomb does not oxidize the tungsten metal; therefore this might explain the lower heat of combustion values on the CA composite in comparison to the theoretical value shown in Figure 15.

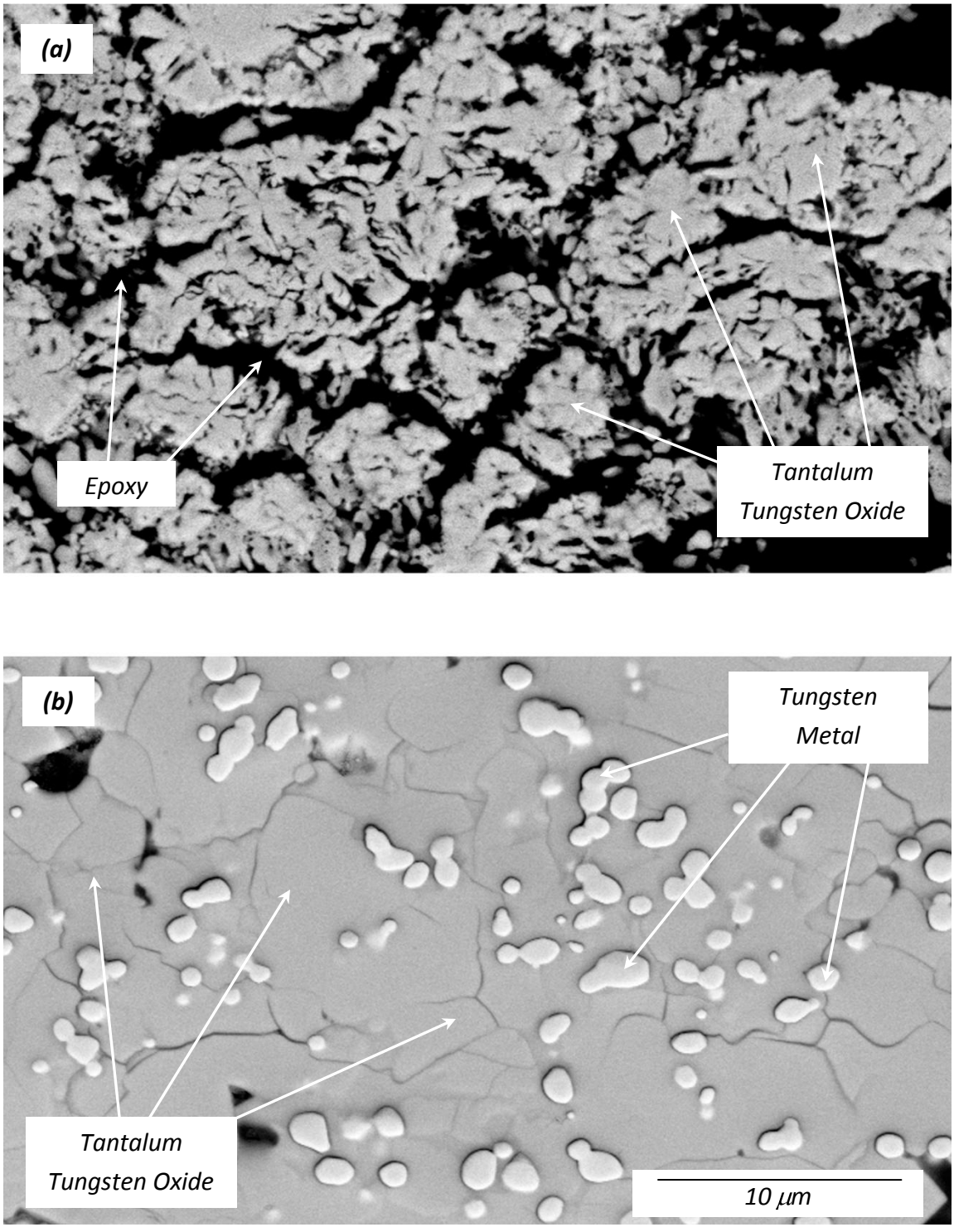

Figure 24: SEM images of post-combustion of a) SG and b) CA powders. Prior to combustion, both samples were consolidated using the HPSPS to 500°C and 300 MPa. The black areas are from the epoxy mount and the medium gray areas are from the complex tantalum-tungsten oxides. EDS analysis determined that the light gray elongated-spheres are tungsten metal particles

3.3 CONCLUSION

The heat of combustion of two distinctly synthesized stoichiometric Ta-WO_3 energetic composites was measured using bomb calorimetry as a function of consolidation temperature. The energetic composites were synthesized using a sol-gel method, which immobilizes the tantalum fuel in a three-dimensional tungsten oxide structure, and by the physical mixing of commercially available nanometric tungsten oxide with tantalum. Density measurements yield similar values for samples consolidated at 400 and 500°C. In contrast, for samples consolidated at 25°C, the measured density is about 10% lower for the composite made from the sol-gel derived tantalum-tungsten oxide composite. The lower density observed in the sol-gel derived composite could be due to the fact this composite is composed of a three-dimensional structure with open porosity which makes it difficult to densify in the absence of applied heat. Moreover, X-ray diffraction patterns show that the amount of pre-reaction between the constituents (Ta and WO_3) increases as a function of consolidation temperature. Such increase in pre-reaction has a direct effect on the measure heat of combustion of the energetic composites. As the pre-reaction increases, the measured energy content decreases for both energetic composites.

LLNL-JRNL-420177

Chapter 4

Activation Energy of Tantalum-Tungsten Oxide Thermite Reactions

4.0 INTRODUCTION

In 1895, German chemist Hans Goldschmidt patented the oxidation/reduction or redox reaction between a metal and a metal oxide, a reaction which has been referred as thermite [59]. A typical thermite reaction is between aluminum and iron oxide,

$$2\,Al + Fe_2O_3 \rightarrow Al_2O_3 + 2Fe + \Delta H \qquad 4\text{-}1$$

where ΔH is the heat released by the reaction. As indicated by Eq (4-1), thermite reactions are exothermic which can be self-sustaining. As a rule, thermite reactions can self-propagate if the adiabatic temperature (T_{ad}) exceeds 1727°C [60]. The T_{ad} for Eq (4-1) has been reported to be 3349°C [1] which is above the required temperature for the reaction to self-propagate. The mechanism of thermite reactions and their utilization have been described in detail elsewhere [1]. Because of the high thermodynamic stability of its oxide (Al_2O_3, ΔH_f = -1675.7 $kJ \cdot mol^{-1}$ at 25°C) and its low melting temperature (660°C), aluminum has been widely used as the fuel metal in combination with various oxides such as

Fe_2O_3, CuO, MoO_3 and WO_3 [7, 8, 24, 25, 31, 61-63]. Important kinetic parameters such as ignition and peak temperatures as related to heating rate are obtained from differential thermal analysis (DTA) and differential scanning calorimetry (DSC) measurements. These temperatures may in turn be use to determine the activation energy of the thermite as a function of a particular parameter of interest (e.g., particle size or distribution).

Determining the activation energy of thermite composites is an important parameter of the ignition process. Such activation energy is defined as the minimum amount of energy required to initiate the reaction between the thermite constituents. Studies have been conducted to determine the activation energy of Al-based thermite composites using isoconversion processing of heat flow data as a function of temperature for various heating rates from DSC measurements [22-24, 26]. In other studies, the activation energy of Al-based intermetallic energetic materials was determined using isoconversion methods from temperature versus time thermograms in laser ignition experiments [64, 65].

The laser ignition of energetic materials is a nonisothermal approach that supplies a constant heat flux to the sample of interest. Such an approach assumes that the ignition temperature corresponds to a fixed state of transformation of the compound from reactants to products. This nonisothermal analysis may be applied to determine the activation energy, E_A, of energetic

materials as long as the thermograms are reproducible and depict specific ignition temperatures [64].

There are a number of isoconversion methods [66-70] that have been applied to determine E_A. According to the Kissinger isoconversion method [16], E_A may be calculated from

$$\frac{d \ln\left[\frac{\beta}{T_{ign}^2}\right]}{dT} = -\frac{E_A}{R} \qquad 4\text{-}2$$

where β is the heating rate, T_{ign} is the ignition temperature, R is the universal gas constant and T is the absolute temperature. The activation energy, E_A, is obtained from the slope of an Arrhenius plot of ln [β / T^2_{ign}] *vs.* 1/T.

As indicated above, several isoconversion methods have been employed to determine E_A, for Al-based thermite reactions from DSC, DTA, and laser ignition measurements [21-23, 26, 64, 65, 71, 72]. To our knowledge, there are no studies on the determination of E_A for thermites involving a high melting fuel metal (~ 3000°C). Here we present results of an investigation on the activation energy of a sol-gel derived Ta-WO_3 thermite reaction. The Kissinger isoconversion method was applied in this study since it has also been previously used on laser ignition studies of intermetallic energetic composites [64, 65].

4.1 EXPERIMENTAL METHODS

4.1.1 Materials Synthesis

A Ta-WO_3 thermite composite powder was prepared using sol-gel techniques. The synthesis of the reactive composite is described in detail elsewhere [73]. Here we provide a brief description of the process: 14.76 g (43.5 mmol) of $WOCl_4$ (F.W. = 339 g $\cdot mol^{-1}$; 98% from Sigma-Aldrich, Milwaukee, WI) were dissolved in 125 mL of an ethanol/H_2O solution with a 95/5 vol % composition. After filtering the solution, 9.2 g (52.2 mmol) of capacitor grade Ta metal powder (H.C. Starck; average particle size 5 μm and 99.99% pure) were added to the filtered solution to make a composite mixture. While stirring the mixture, 20 g (235 mmol) of 3,3,-dimethyloxetane (DMO) (98% pure from Sigma-Aldrich, Milwaukee, WI) were added to the mixture. Shortly thereafter, a gelation of a uniform composite occurred. This method provides an energetic composite that incorporates immobilized micrometric tantalum in a three-dimensional nanostructured tungsten oxide gel with a 6:5 (Ta:WO_3) mole ratio, as shown in Eq. (4-3).

$$6\ Ta + 5\ WO_3 \rightarrow 3\ Ta_2O_5 + 5W \qquad 4\text{-}3$$

4.1.2 Consolidation of Sol-Gel Ta-WO_3

The consolidation of the sol-gel Ta-WO_3 energetic composites was performed using the high-pressure spark plasma sintering (HPSPS) method. Details on this technique are presented elsewhere [36, 37]. HPSPS is similar to

hot-pressing with the distinct difference that the heating is effected by a pulsed DC current applied to the sample and the graphite die. The graphite die assembly is made up of several internal components that allows for the application of pressures as high as 1 GPa. Graphite dies with a 5 mm diameter were used to consolidate the samples at 300 and 400°C. An initial pressure of 150 MPa was applied to the samples which were heated from room temperature to 200°C at approximately 50°C·min^{-1}. In order to remove any residual solvents or physically adsorbed water, the samples were held at 200°C for 2 min. During the 2-min hold, the pressure was increased to 300 MPa and the temperature increased at a rate of approximately 100°C·min^{-1} to the desired final temperature. Once at temperature, the sample was held there for 3 min. The samples had an average weight of 0.225 ± 0.005 g and dimensions of 5.0 ± 0.1 mm diameter by 1.5 ± 0.3 mm height.

4.1.3 Ignition Setup

The development of a custom built ignition setup was necessary since conventional DSC apparatus were not capable of generating the required heating rates to initiate the thermite reaction and since experimental problems were encountered during laser ignition experiments. Laser ignition experiments have been previously applied to the ignition of intermetallic energetic composites [64, 65], therefore laser ignition experiments were attempted to ignite the Ta-WO_3 thermite reaction. The laser experiments generated the required heating rates and initiated the reaction in the composite, but provided irreproducible data. We

found that the thermite sample spalls and disperses away during the laser ignition experiments making it difficult to monitor the temperature profile of the sample. As a result, we built a custom designed apparatus that provided the required heating rates (500 – 2000°C·min^{-1}) and generated reproducible data. In our experimental setup a laser is not used to provide a constant heat flux, instead the sample is exposed to a constant radiant heat flux provided by filament wires capable of generating reproducible thermograms and specific ignition temperatures.

Our experimental setup consisted of placing a 50 mm diameter quartz tube in a tube furnace operating at temperatures ranging from 800 to 1000°C depending on the desired heating rate. One end of the tube furnace was capped with a fitting to allow inert gas to flow through the tube. The other end of the tube remained open to allow for the insertion of a smaller (~ 25 mm diameter) quartz tube assembly (see Figure 25 (a)). The smaller tube (Figure 25(b)) was likewise capped on one end by a fitting to hold the 25 mm quartz tube in place, fasten an alumina tube and allow for inert gas to flow during the ignition experiments. The sample was assembled by attaching a 0.127 mm K-type thermocouple to the top surface of the sample using conductive silver ink (Alfa Aesar, Ward Hill, MA). The sample was then covered with a 0.6 mm thick zirconia blanket to moderate the heat flow to the sample (Figure 25(c)). The thermocouple with the attached sample and zirconia blanket were then inserted through an alumina tube containing two ports for each of the thermocouple leads. Argon gas was purged

at 300 mL·min^{-1} during the experiment. Figure 25 (d) shows a schematic of a fully assembled experimental setup.

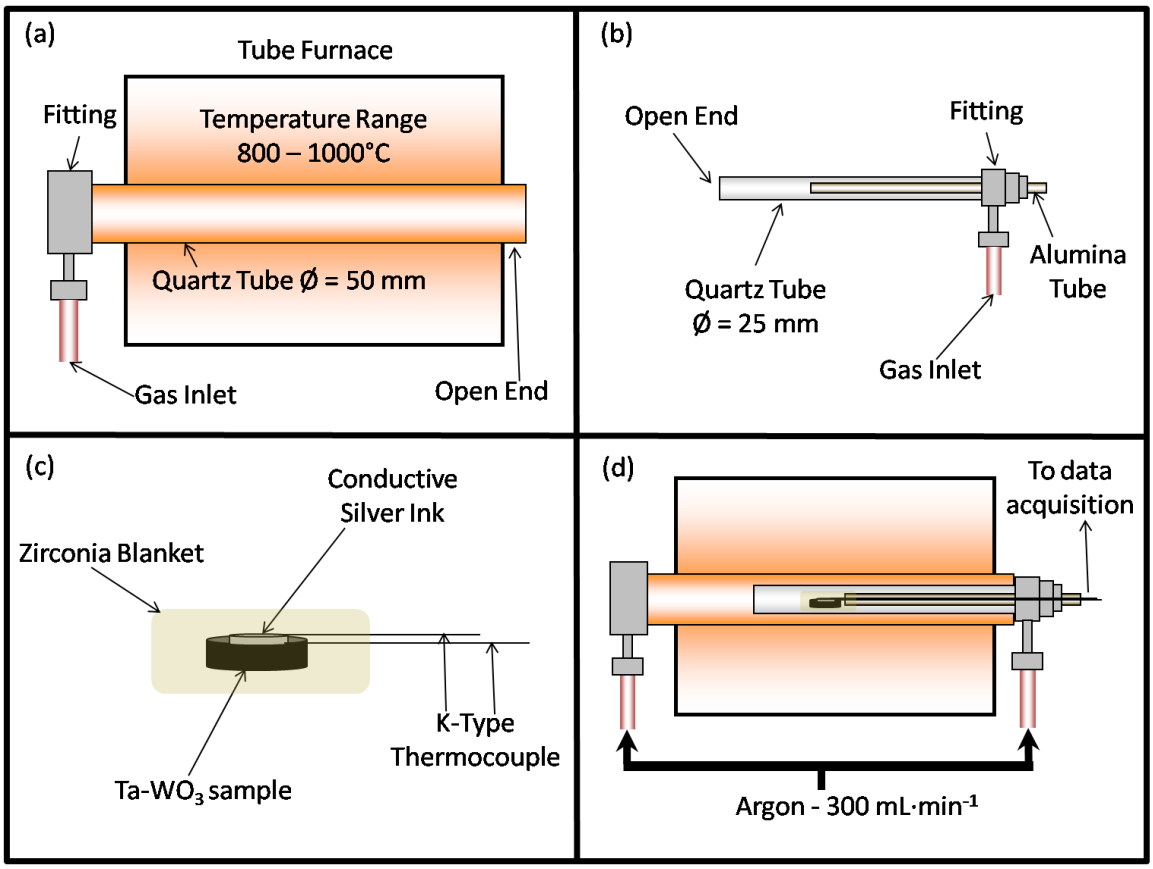

Figure 25: Schematic representation of experimental setup for ignition studies.

At least 10 samples at each consolidation temperature (300 and 400°C) were tested using the described experimental setup. Temperature versus time data were collected at an average rate of 36 µs per data point using an Agilent 34970A Data Acquisition/Switch Unit. Heating rates varied from 500 to 2000°C·min^{-1}.

4.2 RESULTS AND DISCUSSIONS

4.2.1 Ignition Thermograms and Activation Energy

Typical thermograms of samples consolidated at 300 and 400°C by the HPSPS method are presented in Figure 26. The main ignition temperature will be defined as the last sharp temperature rise observed on the thermograms. Such sharp increase in temperature rate will most commonly be in the order of at least 30 x 10^3 °C·min^{-1}. It can be observed that the temperature profile for the sample consolidated at 300°C is different from that of the sample consolidated at 400°C. The sample consolidated at 300°C shows a shoulder in the temperature profile prior to the final rise associated with the ignition of the reaction. In contrast, the sample consolidated at 400°C does not show a similar change in the temperature profile prior to ignition.

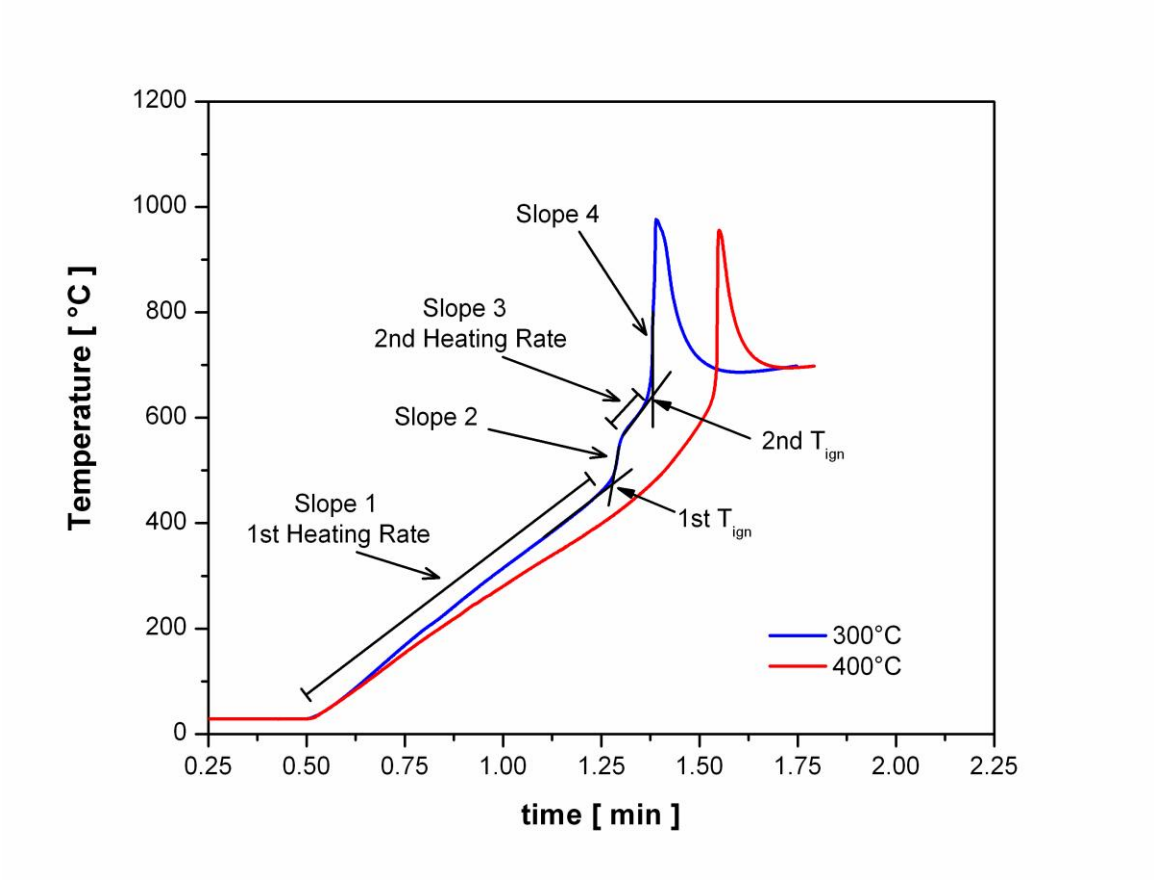

Figure 26: Shows a typical thermogram for Ta-WO_3 samples consolidated at 300 and 400°C. It also presents a schematic on the how the heating rate and the ignition temperature where determined with respect to the thermogram.

The heating rates and the ignition temperatures for each sample were calculated and determined using their corresponding thermograms. Since the 300°C samples displayed a shoulder in the temperature response prior to ignition, two heating rates and two ignition temperatures were calculated and determined for each sample. The first heating rate was calculated for the temperature rise from room temperature to the beginning of the temperature shoulder (labeled as Slope 1 in Figure 26). The first ignition temperature was determined from the intersection of a tangent line between Slope 1 and Slope 2

(Slope 2 represents the initial part of the shoulder, as shown in Figure 26). The first heating rate and ignition temperature for the 300°C samples in Figure 26 were calculated and determined to be approximately 588°C·min^{-1} and 478°C, respectively. From hereafter we will refer to this as the 1st ignition data for the 300°C thermograms. The second heating rate was calculated from Slope 3 as indicated in Figure 26. The second ignition temperature was determined from the intersection of a tangent line drawn between Slope 3 and Slope 4. The second heating rate and ignition temperature for the 300°C samples in Figure 26 were determined to be approximately 927°C·min^{-1} and 533°C, respectively. From hereafter we will refer to this as the 2nd ignition data for the 300°C thermograms.

The same methodology was applied to calculate and determine the heating rate and ignition temperature for the 400°C samples. The difference between the 300°C and the 400°C samples is that for the 400°C samples only one heating rate and one ignition temperature were determined. Such distinction was necessary since these samples do not undergo a distinct change in temperature response prior to ignition. The heating rate and ignition temperature for the 400°C samples in Figure 26 were calculated to be about 505°C·min^{-1} and 551°C, respectively.

Heating rates generated from our experimental setup to initiate the Ta-WO_3 thermite reaction ranged from about 500 to 2000°C·min^{-1} and the ignition temperatures ranged from approximately 465 to 670°C. All of the heating rates

and ignition temperatures were applied to the Kissinger isoconversion method to determine the activation energy, E_A, of the samples consolidated at each temperature. Table 3 shows the calculated activation energy values for SG derived Ta-WO_3 samples consolidated at 300 and 400°C. It can be seen from the root mean square values, the uncertainty in the calculated activation energy for the first ignition data is high. The root mean square is the certainty on the best fit line through the data points. A root mean square value close to unity reflects a higher certainty. A low root mean square value corresponds to a low certainty or high uncertainty. We postulate that this uncertainty may be related to complex pre-ignition reactions between the constituents. Pre-ignition reactions have been verified by previous observations in intermetallic energetic composites [34].

Table 3: Apparent activation energy values determined by the Kissinger isoconversion method to SG derived Ta-WO_3 samples consolidated at to 300 and 400°C.

Consolidation Temperature [°C]	Activation Energy [$kJ \cdot mol^{-1}$]	Root Mean Square
300	1st Ignition Data 7.544 ± 5.36	0.021
	2nd Ignition Data 37.787 ± 1.58	0.847
400	57.381 ± 2.26	0.943

4.2.2 Ignition Quench of Consolidated 300°C Sol-Gel Ta-WO_3

To determine if pre-ignition reactions do occur in the samples consolidated at 300°C, partially converting of the reactants of the SG derived Ta-WO_3 powders to products or intermediate phases, quenching experiments were carried out. Figure 27 shows the XRD patterns of (a) the starting SG derived Ta-WO_3 powder mixture, (b) sample consolidated at 300°C, (c) sample consolidated at 400°C, and (d) a non-consolidated (as-received) powder mixture of a commercially available WO_3 and Ta. The x-ray diffraction patterns indicate that the WO_3 in the SG derived Ta-WO_3 composite is amorphous as the pattern only shows Ta peaks. In contrast and as expected, the XRD pattern of the powder mixture of the commercially available WO_3 and Ta shows that both constituents are crystalline. In addition, the sample consolidated at 300°C shows minor peaks of tantalum suboxide indicative of pre-ignition reaction between the constituents. The Ta suboxide that best fits these peaks is in the form of TaO_x as indicated by Brauer, et al. [56]. Furthermore, Figure 27 (b) shows that the phase WO_3 remains amorphous. In contrast, the XRD of the sample consolidated at 400°C shows a higher degree of pre-ignition reaction between the Ta and the WO_3 as can be seen by the intensity of the tantalum suboxide peaks, Figure 27 (c). In this case, there is evidence of the initiation of the crystallization of the amorphous WO_3 as indicated by the presence of two peaks labeled WO_3 in the XRD pattern (Figure 27 (c)).

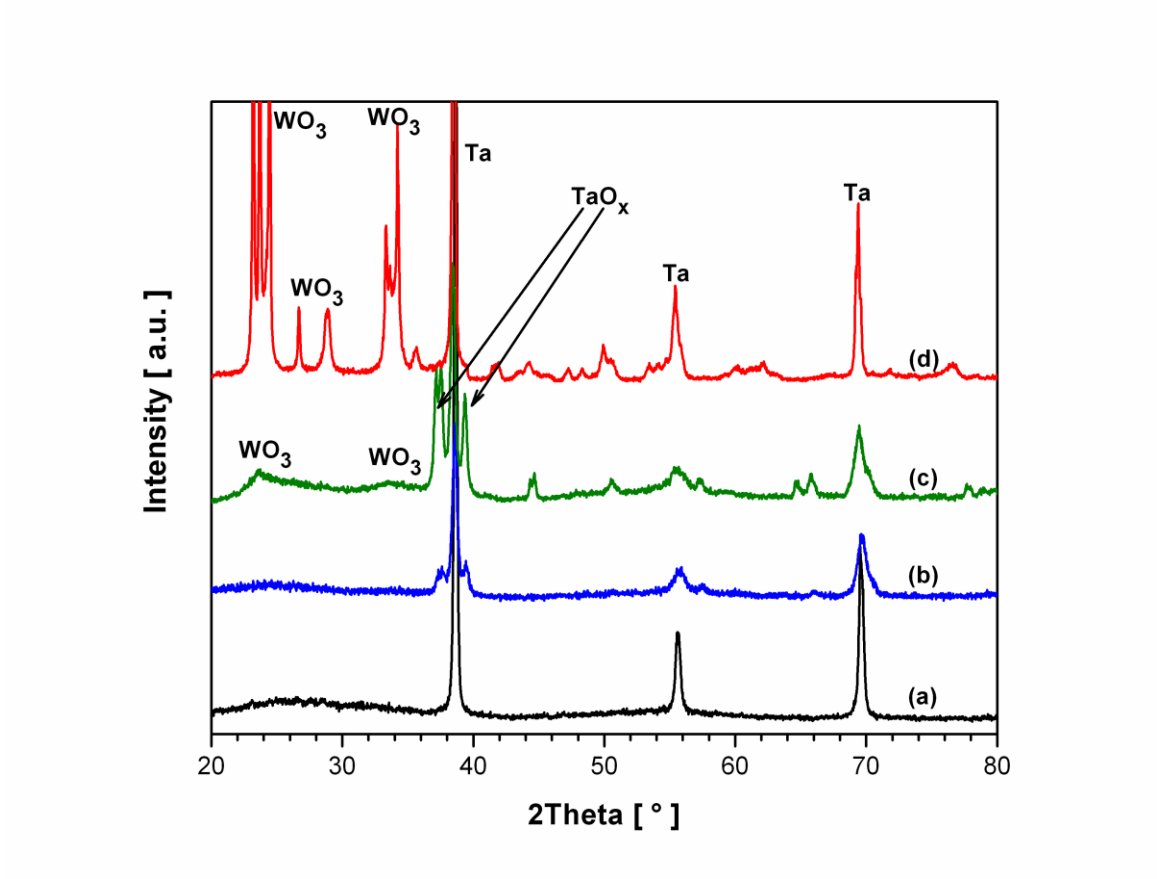

Figure 27: XRD patterns of (a) the starting SG derived Ta-WO_3 powder, (b) a 300°C as-consolidated SG Ta-WO_3 ground powder sample, (c) a 400°C as-consolidated SG Ta-WO_3 ground powder sample and (d) a non-consolidated (as-received) powder mixture of a commercially available WO_3 and Ta. The 300 and 400°C samples were consolidated using the HPSPS.

To investigate the sequence of phase formation in the thermite reaction, samples were quenched by rapidly removing them from the tube furnace prior to ignition**.** Figure 28 shows typical thermograms of the sample sintered at 300°C. Curve 1 is the typical temperature profile for an unquenched sample while curve 2 shows a thermogram of the quenched sample. The quenching (quick removal of the sample from the hot zone) resulted in the cessation of interactions prior to

the main combustion reaction. The approximate heating and cooling rates for this sample were 590°C·min^{-1} and 335°C·min^{-1}, respectively.

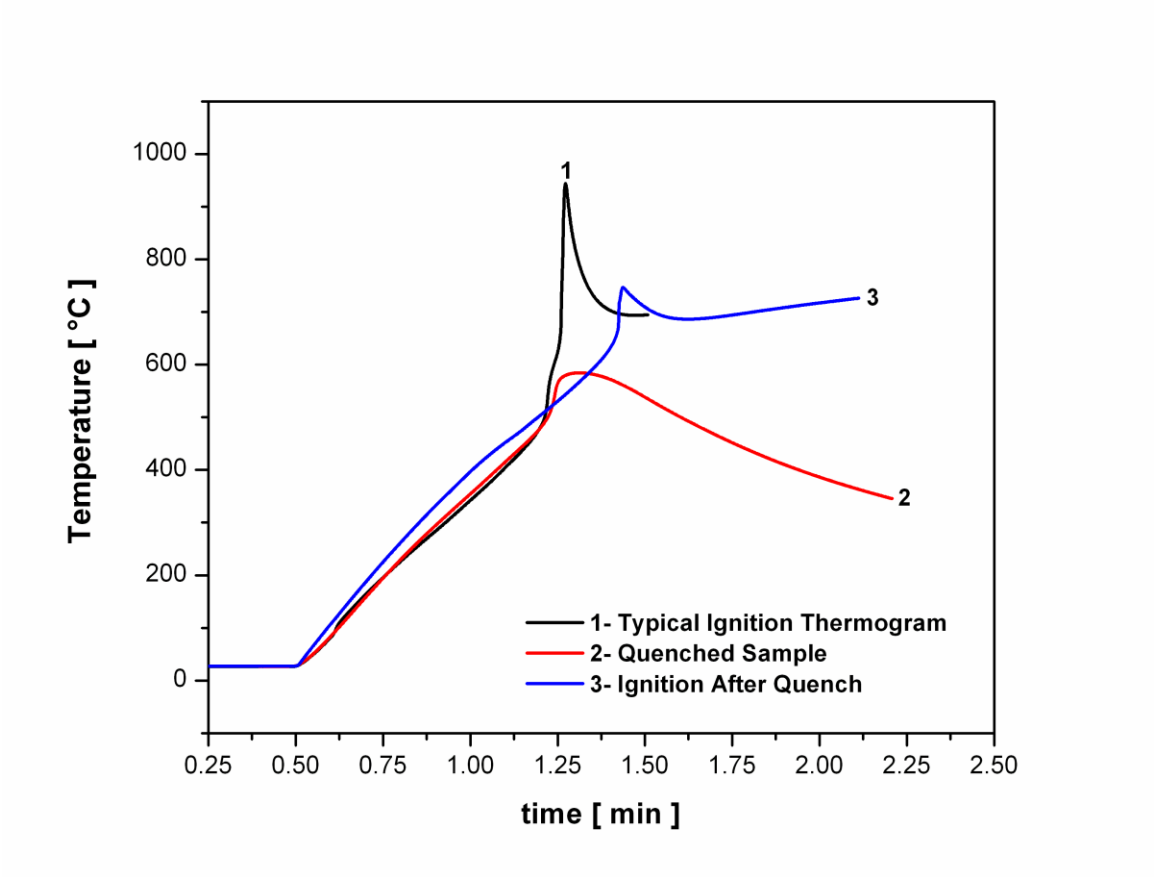

Figure 28: Thermograms for (1) a typical ignition for a 300°C SG Ta-WO_3, (2) ignition quench of a 300°C SG Ta-WO_3 and (3) the ignition of the quenched 300°C SG Ta-WO_3 sample.

To be used as a reference point, Figure 29 (a) shows the XRD pattern of the SG-derived Ta-WO_3 sample consolidated at 300°C. It can be observed that this sample is composed of crystalline Ta, TaO_x, and amorphous WO_3. Figure 29 (b) shows the XRD pattern of the quenched SG-derived Ta-WO_3 sample consolidated at 300°C. XRD analysis of the quenched sample showed evidence of crystallization of the amorphous WO_3 as indicated by the two peaks labeled as

WO_3, but no significant evidence of pre-ignition reaction is observed, as seen in Figure 29 (b). Furthermore, when the quenched sample (curve 2, Figure 28) was exposed to the same thermal cycle for a second time and allowed to ignite (curve 3, Figure 28), its thermogram does not exhibit a distinct temperature shoulder prior to ignition as the thermograms of the 300°C samples typically do. It is important to point out that the ignition time of the quenched sample (curve 3, Figure 28) is about 12 s longer than the unquenched sample (curve 1, Figure 28). We postulate that the crystallization of the amorphous WO_3 is an exothermic event that acts as an internal heat source that decreases the ignition time. The rapid increase in temperature shown in the thermogram (curve 1, Figure 28) during the crystallization of the WO_3 decreases the ignition time of an unquenched sample (curve 1, Figure 28) in comparison to a quenched sample (curve 3, Figure 28). Therefore, it is concluded that the abrupt change in temperature response (or temperature shoulder) prior to ignition, observed in the thermograms for 300°C Ta-WO_3 samples, is not due to a pre-ignition reaction between the Ta and the WO_3 but instead is due to the crystallization of WO_3 as shown by the x-ray diffraction patterns in Figure 29 (b).

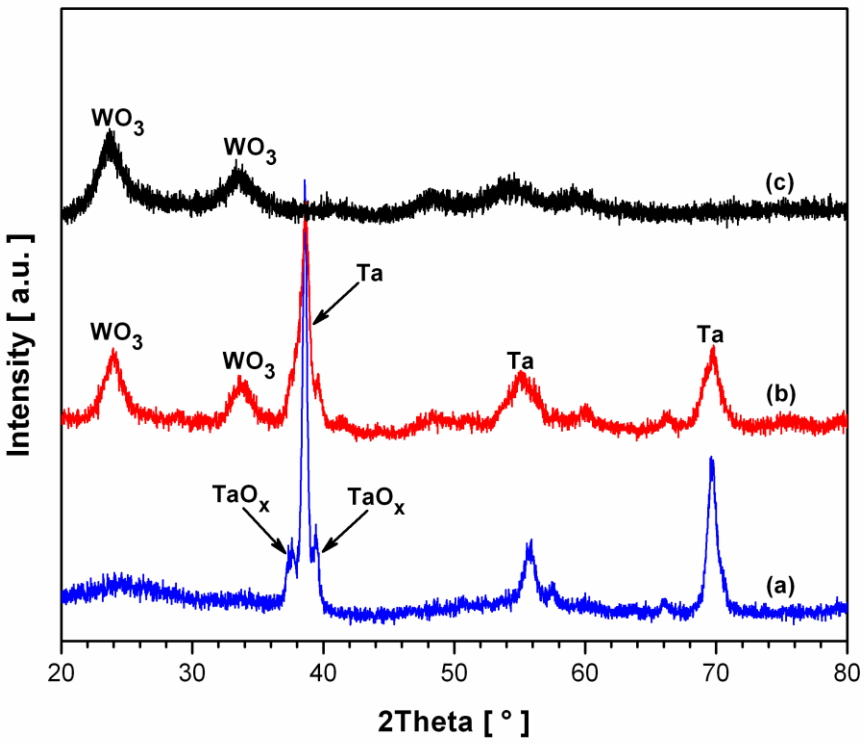

Figure 29: XRD patterns of (a) as-consolidated 300°C SG derived Ta-WO3 pellet using the HPSPS to 300 MPa (b) quenched as-consolidated 300°C SG derived Ta-WO3 pellet using the HPSPS to 300 MPa and (c) a quenched sol-gel amorphous WO_3 pellet pressed at 25°C and 300 MPa.

4.2.3 Ignition Quench of Sol-Gel Amorphous WO_3

To verify that the temperature shoulder response in the 300°C SG Ta-WO_3 samples was due to the crystallization of WO_3, attempts were made to consolidate several sol-gel amorphous WO_3 samples at 300°C using the HPSPS. After several trials, it was evident that such WO_3 samples are difficult to consolidate and in fact crystallize during consolidation. Thus, it was not possible to compare the SG derived Ta-WO_3 samples to sol-gel amorphous WO_3 under similar consolidation conditions. However, pressing a sol-gel amorphous WO_3

sample at 25°C and then quenching it is acceptable since we are able to obtain cylindrical samples and most importantly the sample remains amorphous. Figure 30 shows the thermograms of the quenched SG Ta-WO_3 with a cooling rate of 335°C·min^{-1} and the sol-gel amorphous WO_3 sample with a cooling rate of 225°C·min^{-1}. It can be observed that both samples were quenched at the same temperature; hence making it possible to compare their crystal structure.

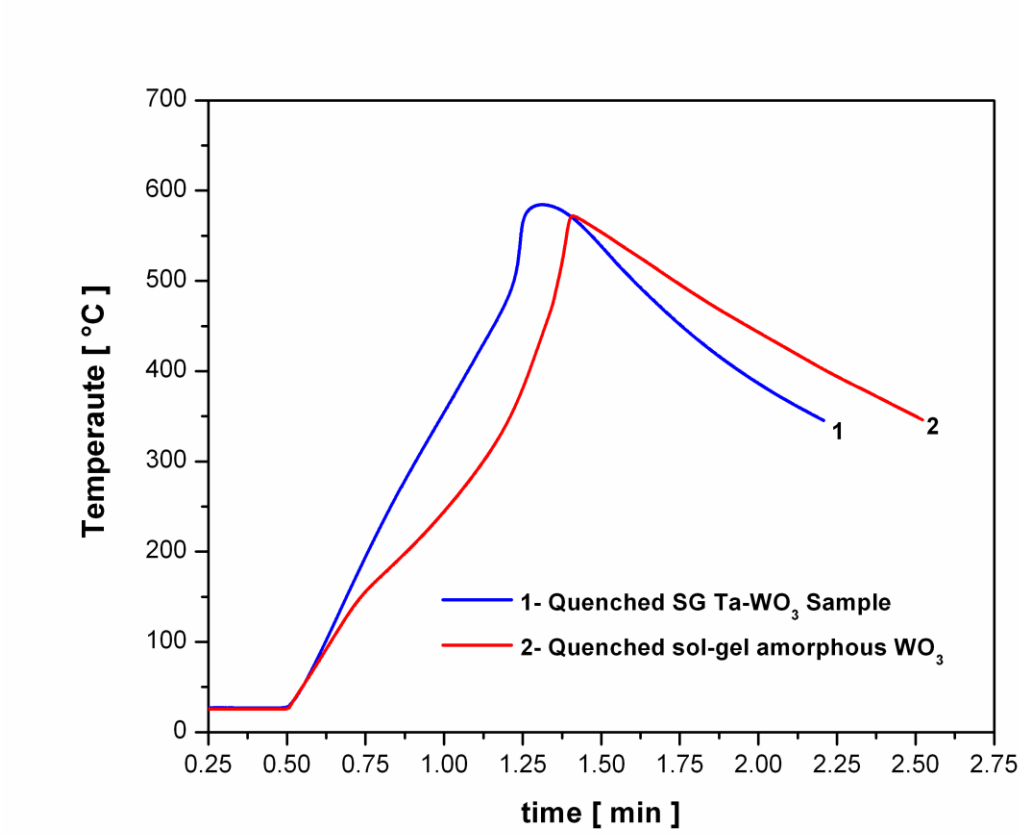

Figure 30: Quenched thermograms of (1) SG Ta-WO_3 and (2) sol-gel amorphous WO_3. The SG Ta-WO_3 sample was pressed to 300°C using the HPSPS and the sol-gel amorphous WO_3 was pressed at 25°C. Both samples were pressed to 300 MPa. Note: Sample 1 was quenched at ~1.25 min (after ~45 sec of heating) and Sample 2 was quenched at ~1.375 min (after ~55 sec of heating).

It is important to note that the difference in heating rate between the SG derived Ta-WO_3 composite and the amorphous WO_3 in Figure 30 may be attributed to differences in thermal conductivity of each sample. During the experiment, the WO_3 will respond slower to the heating as it lacks the thermal response of the Ta. Moreover, the difference may be attributed to the fact that the WO_3 is a porous three-dimensional nanostructure network whose convective heat transfer will be the rate limiting factor. The XRD pattern of the quenched WO_3 shows that the WO_3 has begun to crystallize as indicated by the two WO_3 peaks in Figure 29 (c). This pattern is very similar to the one obtained from the quenched Ta-WO_3 sample in Figure 29 (b). This supports the proposal that the temperature shoulder on the 300°C samples may be due to the crystallization of WO_3 and not a pre-ignition reaction between the reactants.

4.2.4 Consolidation and Ignition of Ta-WO_3 powder mixture with Crystalline WO_3

To further explore the concept that the temperature shoulder on the 300°C SG derived Ta-WO_3 samples is the consequence of the crystallization of WO_3, experiments were carried out to consolidate Ta-WO_3 energetic composites made with crystalline WO_3 instead of amorphous WO_3 under similar consolidation conditions. In five attempts, only two Ta-WO_3 samples with crystalline WO_3 with similar masses as the samples made with the amorphous WO_3 were produced under similar consolidation conditions. Therefore, from a consolidation point of view, the composite with the amorphous WO_3 consolidates much better than the composite with the crystalline WO_3. The composite with the amorphous WO_3

always produces good samples after each consolidation run. Since consolidating the Ta-WO_3 composite with the crystalline WO_3 was difficult, ignition experiments were performed with smaller mass samples (≤ 0.1 g instead of 0.225 g). It was found that such samples react, but do not ignite under the lowest heating setting (furnace at 800°C). Instead, in order to ignite Ta-WO_3 samples with crystalline WO_3, the furnace was set to 1000°C, which is the highest temperature setting used in these ignition experiments.

Ta-WO_3 samples with crystalline WO_3 of approximately 0.225 g were ignition tested while setting the furnace to 1000°C. Results show (as seen in Figure 31) that the ignition of the Ta-WO_3 with crystalline WO_3 does not exhibit the abrupt change in temperature response prior to ignition as previously observed in the SG derived Ta-WO_3 samples consolidated to 300°C. This may be attributed to the fact that the WO_3 in the Ta-WO_3 composite is already crystalline. These results further support the concept that the abrupt change in temperature response prior to ignition in the Ta-WO_3 samples relates to crystallization of the amorphous WO_3. Furthermore, Figure 31 shows that the ignition of the Ta-WO_3 with the crystalline WO_3 occurs at about 800°C which is about 150°C higher than the Ta-WO_3 with amorphous WO_3 under similar heating conditions. In addition, it is important to note that the ignition time for both samples is very similar. This indicates that at these heating rates, the amount of heat required to ignite these thermite composites is about the same regardless of the crystal structure of the reactants. The differences in heating rates may be

attributed to the fact that the amorphous WO_3 in the sol-gel derived Ta-WO_3 composite is a three dimensional porous gas-trapping nanostructure that results in a good insulating performance, thus reduces the thermal conductivity through the sample. It has been reported that the radiative thermal conductivity of resorcinol-formaldehyde aerogel is significantly lower than its solid thermal conductivity [74]. The gas-trapping nanostructure in the sol-gel derived Ta-WO_3 limits the thermal conductivity of the sample, hence the lower heating rate observed for this sample in Figure 31.

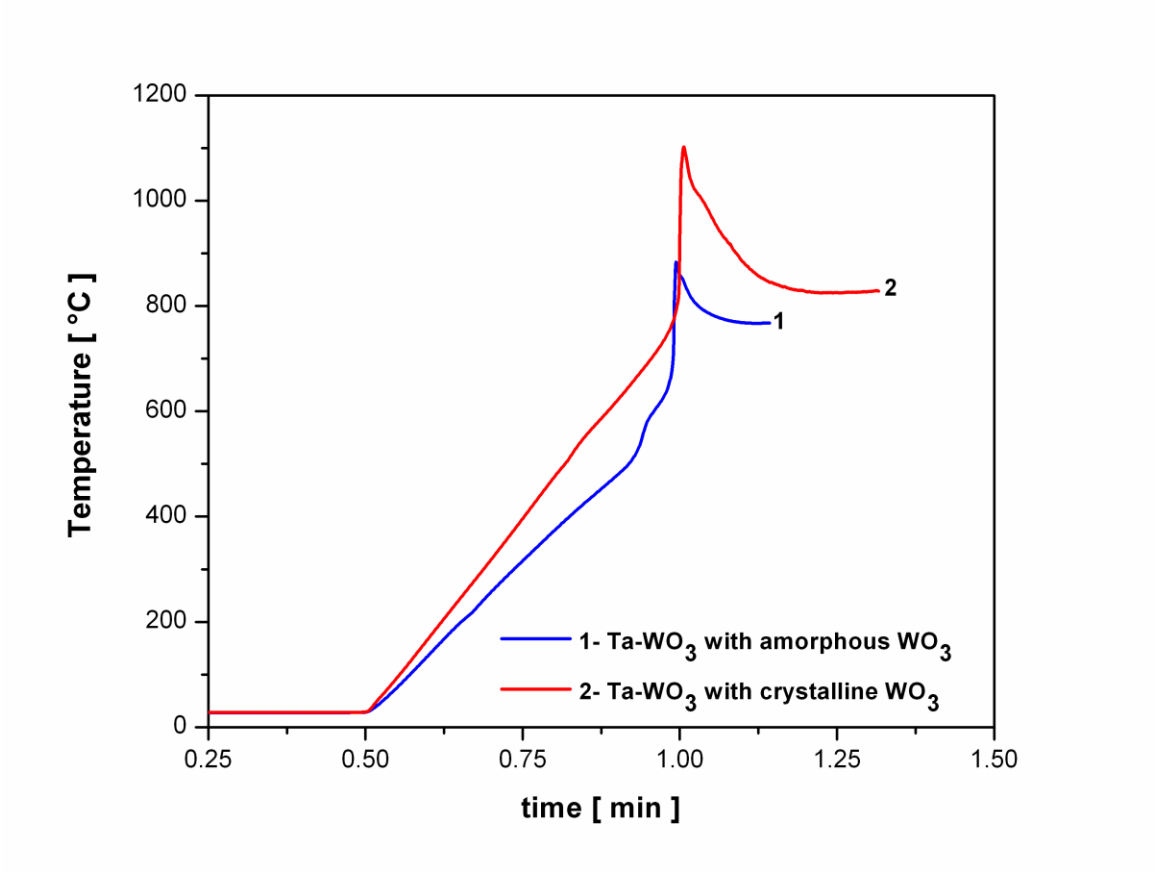

Figure 31: Typical ignition thermograms of (1) SG derived Ta-WO_3 composite and (2) Ta-WO_3 powder mixture with crystalline WO_3 when the furnace temperature is set 1000°C. Both samples were consolidated using the HPSPS to 300°C and 300 MPa.

4.2.5 X-Ray Analysis of Post-Ignition SG Ta-WO_3 powders

X-ray analyses were performed on post-ignition SG Ta-WO_3 powders consolidated to 300 and 400°C. It was found that both powders are best indexed to tantalum oxide and tungsten metal. Figure 32 shows the XRD patterns for samples consolidated to (a) 300°C and (b) 400°C. It can be observed that the crystal structure of the tantalum oxide is different for the post-ignition powders. The crystal structure of the tantalum oxide in the sample consolidated to 300°C is orthorhombic and for the sample consolidated to 400°C is triclinic. The differences in the crystal structure may be attributed to the fact that each sample has a different degree of pre-reaction before the ignition experiments as shown in Figure 27.

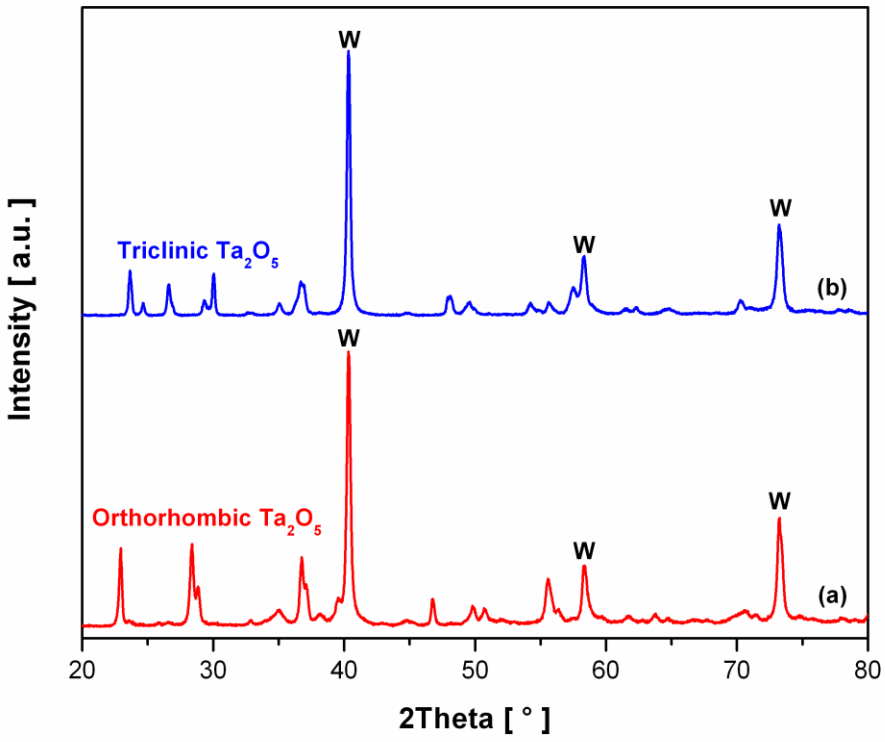

Figure 32: XRD patterns of post-ignition SG Ta-WO_3 powders consolidated to (a) 300°C and (b) 400°C using the HPSPS with an applied pressure of 300 MPa. Both samples are composed of tantalum oxide and tungsten metal (as shown by the W labels on the patterns). The unlabeled peaks in (a) and (b) are best indexed to orthorhombic tantalum oxide and triclinic tantalum oxide, respectively.

4.3 CONCLUSIONS

The activation energy of a tantalum-tungsten oxide thermite composite was determined using the Kissinger isoconversion method. Powder samples were consolidated using the High Pressure Spark Plasma Sintering (HPSPS) technique at 300 and 400°C. A custom built ignition setup was developed to measure ignition temperatures at high heating rates (500 – 2000°C·min^{-1}). Such heating rates were required in order to ignite the thermite composite. Unlike the 400°C samples, results show that the samples consolidated to 300°C undergo an abrupt change in temperature response prior to ignition. This change in temperature response has been attributed to the crystallization of the amorphous WO_3 in the sol-gel derived Ta-WO_3 thermite composite and not to a pre-ignition reaction between the constituents. Ignition temperatures for the Ta-WO_3 thermite ranged from approximately 465 to 670°C. The ignition of Ta-WO_3 with amorphous WO_3 generally occurs at lower temperatures than the Ta-WO_3 composite with the crystalline WO_3. It is postulated that the crystallization of the amorphous WO_3 provides sufficient energy to ignite the 300°C samples at lower temperatures. Moreover, it was found that the amorphous WO_3 used in this study, crystallizes while being consolidated under the same conditions as the Ta-WO_3 thermite composite. This indicates that the consolidation mechanism of the Ta-WO_3 and the sol-gel amorphous WO_3 are different.

LLNL-JRNL-425030

Chapter 5

5.0 CONCLUSION

The synthesis and consolidation of a Ta-WO_3 energetic composite prepared by sol-gel techniques was proposed and successfully achieved. The advantage of the sol-gel derived composite over conventional mixing loose powders is that the sol-gel powder provides a three-dimensional nanostructured network of amorphous WO_3 oxidizer in a gel with immobilized micron-size Ta fuel embedded. Such powder configuration permits for the constituents to be in intimate contact. Due to the energetic nature of the material, the composite was initially prepared with sub-stoichiometric amounts of Ta fuel. In addition, the ignition sensitivity of the composite was tested using common techniques such as impact, friction and drop hammer. Results showed that the composite was not sensitive to any of the ignition techniques. The consolidation of the composite was carried using the High Pressure Spark Plasma Sintering (HPSPS) technique at temperatures ranging from 25 to 500°C. The amorphous nature of the WO_3 oxidizer prior to consolidation allows for the densification of the energetic composite by viscous flow at relatively mild consolidation conditions.

To determine the minimum amount of energy required to initiate the reaction of the energetic composite, the activation energy of a sol-gel derived Ta-WO_3 thermite composite was determined using the Kissinger isoconversion method. After several attempts to initiate the energetic composite using

conventional DSC apparatus or high energy laser ignition, a custom built ignition setup was developed to ignite and measure the ignition temperatures. Unlike the 400°C samples, results show that the samples consolidated to 300°C undergo an abrupt change in temperature response prior to ignition. This change in temperature response has been attributed to the crystallization of the amorphous WO_3 in the sol-gel derived Ta-WO_3 thermite composite and not to a pre-ignition reaction between the constituents. The abrupt change in temperature response prior to ignition is not observed in the 400°C samples since the amorphous WO_3 in the thermite composite crystallizes during the consolidation process.

To measure the amount of energy release by the Ta-WO_3 thermite composite in an oxygen rich atmosphere, the heat of combustion of a fully stoichiometric sol-gel derived Ta-WO_3 thermite composite was measured using bomb calorimetry as a function of consolidation temperature and relative density. To compare the performance of the sol-gel derived composite in terms of its energy released, a commercially available nanometric WO_3 was physical mixed with micrometric tantalum powder. Such powder was consolidated using the same parameters as the sol-gel derived and its energy release was measured using the bomb calorimetry technique. Density measurements showed that the sol-gel composite yields higher values than the commercially available composite for samples consolidated at 400 and 500°C. In contrast, for samples consolidated at 25°C, the measured density is about 6% lower for the sol-gel composite than the commercially available composite. X-ray diffraction analyses showed that the amount of pre-reaction increases as a function of consolidation

temperature. As the pre-reaction increases, the measured energy release decreases for both energetic composites.

Energy release results showed that the sol-gel derived composite releases higher amounts of energy than its counterpart the commercially available composite. The higher release of energy was attributed to the fact that the sol-gel derived Ta-WO_3 thermite composite contained 2.52 wt% carbon.

6.0 REFERENCES

1. Wang, L.L., Z.A. Munir, and Y.M. Maximov, *Thermite Reactions - Their Utilization in the Synthesis and Processing of Materials.* Journal of Materials Science, 1993. **28**(14): p. 3693-3708.

2. Mohler, J.H., D.L. Halcomb, and D.R. Begeal. *15th International Pyrotechnics Seminar*. 1990. Illinois Institute of Technology, Chicago, IL.

3. Kelster, F.Z. and G.S. Smelker. June 26, 1976: U.S. Patent 3,742,129.

4. Dixson, G.P., J.A. Martin, and D. Thomson. February 10, 1998: U.S. Patent 5,717,159.

5. Giles, J., *Green explosives: Collateral damage.* Nature, 2004. **427**(6975): p. 580-581.

6. Montgomery, H.E. June 8, 1976: U.S. Patent 3,961,576.

7. Prentice, D., M.L. Pantoya, and A.E. Gash, *Combustion wave speeds of sol-gel-synthesized tungsten trioxide and nano-aluminum: The effect of impurities on flame propagation.* Energy & Fuels, 2006. **20**(6): p. 2370-2376.

8. Plantier, K.B., M.L. Pantoya, and A.E. Gash, *Combustion wave speeds of nanocomposite Al/Fe2O3: the effects of Fe2O3 particle synthesis technique.* Combustion and Flame, 2005. **140**(4): p. 299-309.

9. Chen, D.M., et al., *Combustion Behavior and Thermophysical Properties of Metal -Based Solid Fuels.* Journal of Propulsion and Power, 1991. **7**(2): p. 250-257.

10. Ames, R.G. 2006, Materials Research Society Symposium Proceedings. p. 0896-H93-08.1.

11. Clement, D., et al., *Highly explosive nanosilicon-based composite materials.* Physica Status Solidi a-Applications and Materials Science, 2005. **202**(8): p. 1357-1364.

12. Dyer, T.S. and Z.A. Munir, *The Synthesis of Nickel Aluminides by Multilayer Self-Propagating Combustion.* Metallurgical and Materials Transactions B-Process Metallurgy and Materials Processing Science, 1995. **26**(3): p. 603-610.

13. Dyer, T.S., Z.A. Munir, and V. Ruth, *The Combustion Synthesis of Multilayer Nial Systems.* Scripta Metallurgica Et Materialia, 1994. **30**(10): p. 1281-1286.

14. Blobaum, K.J., et al., *Deposition and characterization of a self-propagating CuOx/Al thermite reaction in a multilayer foil geometry.* Journal of Applied Physics, 2003. **94**(5): p. 2915-2922.

15. Schoenitz, M., T.S. Ward, and E.L. Dreizin. *Fully dense nano-composite energetic powders prepared by arrested reactive milling*. in *30th International Symposium on Combustion*. 2004. Chicago, IL: Combustion Inst.

16. Dreizin, E.L. and M. Schoenitz, *Nano-Composite Energetic Powders Prepared by Arrested Reactive Milling*. Published in March 2006: United States of America.

17. Schoenitz, M., T. Ward, and E.L. Dreizin, Mater. Res. Soc. Symp. Proc., 2004. **800**: p. AA2.6.1 - AA2.6.6.

18. Kuntz, J.D., et al., *Tantalum-Tungsten Oxide Thermite Composites Prepared by Sol-Gel Synthesis and Spark Plasma Sintering.* Chemistry of Materials, 2009.

19. Gash, A.E., et al. *New sol-gel synthetic route to transition and main-group metal oxide aerogels using inorganic salt precursors*. in *6th International Symposium on Aerogels (ISA-6)*. 2000. Albuquerque, New Mexico.

20. Tillotson, T.M., et al. *Nanostructured energetic materials using sol-gel methodologies*. in *6th International Symposium on Aerogels (ISA-6)*. 2000. Albuquerque, New Mexico.

21. Fan, R.H., et al., *Kinetics of thermite reaction in Al-Fe2O3 system.* Thermochimica Acta, 2006. **440**(2): p. 129-131.

22. Dyer, T. and Z. Munir, *The synthesis of nickel aluminides by multilayer self-propagating combustion.* Metallurgical and Materials Transactions B, 1995. **26**(3): p. 603-610.

23. Sun, J., M.L. Pantoya, and S.L. Simon, *Dependence of size and size distribution on reactivity of aluminum nanoparticles in reactions with oxygen and MoO3.* Thermochimica Acta, 2006. **444**(2): p. 117-127.

24. Pantoya, M.L. and J.J. Granier. *The effect of slow heating rates on the reaction mechanisms of nano and micron composite thermite reactions*. in

33rd Annual Meeting of the North-American-Thermal-Analysis-Society. 2005. Univ City, CA: Springer.

25. Umbrajkar, S.M., M. Schoenitz, and E.L. Dreizin, *Exothermic reactions in Al-CuO nanocomposites.* Thermochimica Acta, 2006. **451**(1-2): p. 34-43.

26. Blobaum, K.J., et al., *Al/Ni formation reactions: characterization of the metastable Al9Ni2 phase and analysis of its formation.* Acta Materialia, 2003. **51**(13): p. 3871-3884.

27. Perry, W.L., et al., *Nano-scale tungsten oxides for metastable intermolecular composites.* Propellants Explosives Pyrotechnics, 2004. **29**(2): p. 99-105.

28. Perry, W.L., et al., *Energy release characteristics of the nanoscale aluminum-tungsten oxide hydrate metastable intermolecular composite.* Journal of Applied Physics, 2007. **101**(6).

29. Bockmon, B.S., et al., *Combustion velocities and propagation mechanisms of metastable interstitial composites.* Journal of Applied Physics, 2005. **98**(6): p. 7.

30. Shoshin, Y.L., et al., *Ignition of aluminum-rich Al-Ti mechanical alloys in air.* Combustion and Flame, 2006. **144**(4): p. 688-697.

31. Schoenitz, M., S. Umbrajkar, and E.L. Dreizin, *Kinetic analysis of thermite reactions in Al-MoO3 nanocomposites.* Journal of Propulsion and Power, 2007. **23**(4): p. 683-687.

32. Stamatis, D., et al., *Fully Dense, Aluminum-Rich Al-CuO Nanocomposite Powders for Energetic Formulations.* Combustion Science and Technology, 2009. **181**(1): p. 97-116.

33. Cashdollar, K.L. and M. Hertzberg, *20-L EXPLOSIBILITY TEST CHAMBER FOR DUSTS AND GASES.* Review of Scientific Instruments, 1985. **56**(4): p. 596-602.

34. Lee, S.-H., et al., *Effect of heating rate on the combustion synthesis of intermetallics.* Materials Science and Engineering A, 2000. **281**(1-2): p. 275-285.

35. Mileham, M.L., M.P. Kramer, and A.E. Stiegman, *Laser initiation processes in thermite energetic materials using laser desorption ionization time-of-flight mass spectrometry.* Journal of Physical Chemistry C, 2007. **111**(45): p. 16883-16888.

36. Munir, Z.A., U. Anselmi-Tamburini, and M. Ohyanagi, *The effect of electric field and pressure on the synthesis and consolidation of materials: A review of the spark plasma sintering method.* Journal of Materials Science, 2006. **41**(3): p. 763-777.

37. Anselmi-Tamburini, U., J.E. Garay, and Z.A. Munir, *Fast low-temperature consolidation of bulk nanometric ceramic materials.* Scripta Materialia, 2006. **54**(5): p. 823-828.

38. Thadhani, N.N., et al., eds. *Multifunctional Energetic Materials*. Vol. 896. 2006, Materials Research Society Symposium Proceedings.

39. Blobaum, K.J., et al., *Investigating the reaction path and growth kinetics in CuOx/Al multilayer foils.* Journal of Applied Physics, 2003. **94**(5): p. 2923-2929.

40. Roine, A., *HSC Chemistry 4.0.* Outokumpu Research Oy.

41. Tillotson, T.M., et al., *Nanostructured energetic materials using sol-gel methodologies.* Journal of Non-Crystalline Solids, 2001. **285**(1-3): p. 338-345.

42. Morris, C.A., et al., *Silica sol as a nanoglue: Flexible synthesis of composite aerogels.* Science, 1999. **284**(5414): p. 622-624.

43. Gash, A.E., et al., *New sol-gel synthetic route to transition and main-group metal oxide aerogels using inorganic salt precursors.* Journal of Non-Crystalline Solids, 2001. **285**(1-3): p. 22-28.

44. Tillotson, T.M., et al., *Sol-gel processing of energetic materials.* Journal of Non-Crystalline Solids, 1998. **225**(1): p. 358-363.

45. Miziolek, A., et al., eds. *Defense Applications of Nanomaterials*. 2004 ACS Symposium Series 891: Washington D.C. 198-210.

46. Prentice, D., M.L. Pantoya, and B.J. Clapsaddle, *Effect of nanocomposite synthesis on the combustion performance of a ternary thermite.* Journal of Physical Chemistry B, 2005. **109**(43): p. 20180-20185.

47. Gash, A.E., et al., *Use of epoxides in the sol-gel synthesis of porous iron(III) oxide monoliths from Fe(III) salts.* Chemistry of Materials, 2001. **13**(3): p. 999-1007.

48. Brunauer, S., P.H. Emmett, and E. Teller, *Adsorption of gases in multimolecular layers.* Journal of the American Chemical Society, 1938. **60**: p. 309-319.

49. Simpson, L.R. and M.F. Foltz, *LLNL Small-Scale Friction Sensitivity (BAM) Test* UCRL-ID-124563 1996.

50. Simpson, L.R. and M.F. Foltz, *LLNL Small-Scale Spark Machine: Static Spark Sensitivity Test*. UCRL-ID 135525 1999.

51. Simpson, L.R. and M.F. Foltz, *LLNL Small-Scale Drop Hammer Impact Sensitivity Test*. UCRL-ID 119665 1995.

52. Kuntz, J.D., et al., *Tantalum-Tungsten Oxide Thermite Composites Prepared by Sol-Gel Synthesis and Spark Plasma Sintering.* Combustion and Flame, 2010. **In-Press**.

53. Daniels, F., *An adiabatic calorimeter.* Journal of the American Chemical Society, 1916. **38**: p. 1473-1480.

54. Shoemaker, D.P., C.W. Garland, and J.W. Nibler, *Experiments in Physical Chemistry.* 1996. **6th Edition**: p. 152 - 158.

55. Hawtin, P., et al., *The Heats of Combustion of Graphite, Diamond and Some Non-Graphitic Carbons.* Philosophical Transactions for the Royal Society of London, Series A, Mathematical and Physical Sciences, 1966. **261**(1116): p. 67-95.

56. Brauer, G., H. Muller, and G. Kuhner, *OXIDE DER TIEFTEMPERATUROXYDATION VON NIOB UND TANTAL.* Journal of the Less-Common Metals, 1962. **4**(6): p. 533-546.

57. Roth, R.S., J.L. Waring, and H.S. Parker, *Effect of oxide additions on the polymorphism of tantalum pentoxide. IV. The system Ta2O5---Ta2WO8.* Journal of Solid State Chemistry, 1970. **2**(3): p. 445-461.

58. Maille, L., et al. *Structure and morphological study of nanometer W and W3O thin films*. in *Symposium on Growth and Evolutio of Ultra Thin Films held at the 2000 European-Materials-Research-Society Spring Meeting*. 2000. Strasbourg, France: Elsevier Science Sa.

59. Goldschmidt, H. 1895: German Patent 96,317.

60. Munir, Z.A., *SYNTHESIS OF HIGH-TEMPERATURE MATERIALS BY SELF-PROPAGATING COMBUSTION METHODS.* American Ceramic Society Bulletin, 1988. **67**(2): p. 342-349.

61. Umbrajkar, S.M., et al. *Aluminum-rich Al-MoO3 nanocomposite powders prepared by arrested reactive milling*. in *AIAA 45th Aerospace Sciences Meeting and Exhibit*. 2007. Reno, NV: Amer Inst Aeronaut Astronaut.

62. Moore, K. and M.L. Pantoya, *Combustion of environmentally altered molybdenum trioxide nanocomposites.* Propellants Explosives Pyrotechnics, 2006. **31**(3): p. 182-187.

63. Son, S.F., et al., *Combustion of nanoscale Al/MoO3 thermite in microchannels.* Journal of Propulsion and Power, 2007. **23**(4): p. 715-721.

64. Hunt, E.M. and M.L. Pantoya, *Ignition dynamics and activation energies of metallic thermites: From nano- to micron-scale particulate composites.* Journal of Applied Physics, 2005. **98**(3): p. 034909.

65. Monagheddu, M., et al., *Ignition phenomena in combustion synthesis: An experimental methodology.* Journal of Applied Physics, 2002. **92**(1): p. 594-599.

66. Kissinger, H.E., *Reaction Kinetics in Differential Thermal Analysis.* Analytical Chemistry, 1957. **29**(11): p. 1702-1706.

67. Ozawa, T., Bull. Chem. Soc. Jpn., 1965. **38**: p. 1881.

68. Flynn, J.H. and L.A. Wall, J. Res. Nat. Bur. Standards, 1966. **70A**: p. 487.

69. Starink, M.J., *A new method for the derivation of activation energies from experiments performed at constant heating rate.* Thermochimica Acta, 1996. **288**(1-2): p. 97-104.

70. Vyazovkin, S., *Advanced isoconversional method.* Journal of Thermal Analysis and Calorimetry, 1997. **49**(3): p. 1493-1499.

71. Wang, Y., et al., *Thermal performance investigation of core-shell Cu/Al micron-nano composites with WO3.* Acta Physico-Chimica Sinica, 2007. **23**(11): p. 1753-1759.

72. Umbrajkar, S.M., et al., *On problems of isoconversion data processing for reactions in Al-rich Al-MoO3 thermites.* Thermochimica Acta, 2008. **477**(1-2): p. 1-6.

73. Kuntz, J.D., O.G. Cervantes, A.E.Gash, and Z.A. Munir, Combustion and Flame, 2010. **In-Press**.

74. Hrubesh, L.W. and R.W. Pekala, *THERMAL-PROPERTIES OF ORGANIC AND INORGANIC AEROGELS.* Journal of Materials Research, 1994. **9**(3): p. 731-738.